Immunoblotting. Mouse tissues were homogenized in buffer containing 50 mM Tris–HCl (pH 8.0), 150 mM NaCl, 1% Nonidet P-40, 0.5% deoxycholate, 0.1% SDS and 1 mM 2-mercaptoethanol with 1 mM phenylmethylsulphonyl fluoride and 6 μg ml^{-1} aprotinin and then centrifuged at 2,500 *g* for 15 min. Equal amounts of protein were separated by 5–20% SDS/PAGE and transferred to Hybond-P membranes (GE Healthcare, Piscataway, NJ, USA). The primary antibodies and their dilutions were as follows: AR (N20, 1:1,000; Santa Cruz Biotechnology, Santa Cruz, CA, USA), Hsp72 (1:1,000; Stressgen Biotechnologies, Victoria, Canada), Hsp40 (1:5,000; Stressgen), Hsp90 (1:1,000; Stressgen), Hsp105 (1:250; Novocastra Laboratories, Newcastle, UK), Hsf-1 (1:5,000; Stressgen), ChAT (1:1,000; Millipore, Billerica, MA, USA), NF-YA (G-2, 1:500; Santa Cruz Biotechnology), SP1 (PEP2, 1:2,000; Santa Cruz Biotechnology), TBP (N-12, 1:500; Santa Cruz Biotechnology) and p53 (DO-1, 1:500, Santa Cruz Biotechnology). Primary antibody binding was probed with horseradish peroxidase-conjugated secondary antibodies at a dilution of 1:5,000, and bands were detected by using an immunoreaction-enhancing solution (Can Get Signal; Toyobo, Osaka, Japan) and enhanced chemiluminescence (ECL Plus; GE Healthcare). An LAS-3000 imaging system (Fujifilm, Tokyo, Japan) was used to produce digital images. The signal intensities of these independent blots were quantified using IMAGE GAUGE software version 4.22 (Fuji) and expressed in arbitrary units. The membranes were reprobed with an anti-GAPDH (1:5,000; Santa Cruz Biotechnology) antibody for normalization.

Histology and immunohistochemistry. Mice deeply anesthetized with pentobarbital were perfused with 4% paraformaldehyde fixative in phosphate buffer (pH 7.4). The tissues were dissected, post-fixed in 10% phosphate-buffered formalin and processed for paraffin embedding. Sections to be stained with an anti-polyglutamine antibody (1C2) were treated with formic acid for 5 min at room temperature; those to be incubated with an anti-HSF-1 antibody were boiled in 10 mM citrate buffer for 15 min. The primary antibodies and their dilutions were as follows: polyglutamine (1:20,000; Millipore), Hsp72 (1:500; Stressgen), anti-HSF-1 (1:5,000; Stressgen), ChAT (1:1,000; Millipore), GFAP (1:2,000; Epitomics, Burlingame, CA, USA), NF-YA (H-209, 1:500; Santa Cruz Biotechnology), SP1 (PEP2, 1:2,000; Santa Cruz Biotechnology), TBP (N-12, 1:500; Santa Cruz Biotechnology), and p53 (DO-1, 1:500; Santa Cruz Biotechnology). Primary antibody binding was probed with a secondary antibody labelled with a polymer as part of the Envision + system containing horseradish peroxidase (Dako Cytomation, Gostrup, Denmark).

Lentiviral vector construct preparation. The cds portion of human *HSF-1* complementary DNA[33] was subcloned into the pEGFP expression vector through *Age1* and *Xho1* restriction sites. *hHSF-1-GFP* was inserted into the pENTR/D/TOPO vector (Invitrogen, Carlsbad, CA) and transferred into the pLenti CMV Neo DEST #2 (705-1) vector, a gift from Dr Eric Campeau (Resverlogix Corp.), using the Gateway system (Invitrogen).

Viral production. Lentivirus was prepared following Campeu's protocol[52]. Briefly, lentiviral particles were produced in HEK293FT cells by transfection using Lipofectamine 2000 (Invitrogen). The lentiviral-containing supernatant was collected 48 h after transfection, and concentrated by ultracentrifugation. The viral titre was measured using Lenti-X qRT-PCR Titration Kit (Clontech, Mountain View, CA).

Injection procedures. Recombinant lentiviral vector expressing hHSF1-GFP or GFP alone (6.7×10^8 copies per μl) was stereotaxically injected into the right motor cortex and striatum (1 μl per 10 min) of 8-week-old AR-97Q mice deeply anethetized with pentobarbital, using a Hamilton syringe (Hamilton, Reno, NV, USA) and a microinjection cannula (Eicom, Kyoto, Japan) as described in Supplementary Method.

Quantitative analysis of immunohistochemistry. To assess 1C2-positive cells, we prepared at least 100 consecutive 6-μm-thick axial sections of the thoracic spinal cord, coronal sections of the cerebrum and cerebellum, and longitudinal sections of skeletal muscle, and immunostained every tenth section with an anti-1C2 antibody. The number of 1C2-positive cells was counted in all of the motor neurons within the anterior horn of the ten axial sections from the thoracic spinal cord and more than 500 neurons in five randomly selected X400 microscopic fields of the ten sections in each region from the cerebrum and cerebellum of each group of mice ($n = 3$) under a light microscope (Bx51; Olympus, Tokyo, Japan). The frequency of 1C2-positive cells was expressed as the number per 100 neurons. For the assessment of 1C2-positive cells in skeletal muscle, the number of 1C2-positive cells was calculated for more than 500 fibres in randomly selected areas of the ten axial sections and the results were expressed as the number per 100 muscle fibres. To measure the number of 1C2-positive cells in the liver and pituitary gland, more than 500 cells in randomly selected areas of the ten axial sections were investigated and the results were expressed as the number per 100 cells. For the quantification of the expression levels of Hsf-1, Nfya, p53, Tbp and Sp1, we performed immunohistochemistry on every 20th section from the 100 consecutive sections. We measured the intensity of nuclear immunoreactivity for each molecule in the anterior horn of the five axial sections from the thoracic spinal cord and more than 500 cells in five randomly selected X400 microscopic fields of the five sections from the cerebral motor and visual cortex, striatum, and cerebellar Purkinje and granule cells from each group of mice ($n = 3$) using an image analyser (WinROOF; Mitani Corporation, Tokyo, Japan). We also measured the intensity of immunoreactivity in the ependymal cells of each section as a standard control, and calculated the signal intensity ratio using this control. To quantify the cell size of motor neurons and the region of anti-GFAP immunoreactivity in the spinal anterior horn, we analysed every tenth section of the 50 consecutive 6-μm-thick axial sections from the thoracic spinal cord using an image analyser (WinROOF). For the purposes of calculating the cell size of hepatocytes, cerebellar Purkinje cells, striatal neurons and cerebral cortex neurons, more than 500 neurons and 1000 hepatocytes in randomly selected areas were examined using an image analyser (WinROOF). To analyse the pathological change in the brain with the lentivirus injection, we prepared consecutive 3-μm-thick coronal sections of the cerebrum and immunostained every five sections with 1C2 and anti-Hsf-1 antibodies. The number of 1C2-positive cells was counted in more than 300 neurons in a X400 microscopic fields around the lentivirus injection site from the five sections under a light microscope (Bx51; Olympus, Tokyo, Japan). We measured the intensity of nuclear immunoreactivity for Hsf-1 in more than 300 cells in X400 microscopic fields using an image analyser (WinROOF).

NMJ staining. 30 μm-thick frozen longitudinal sections of the gastrocnemius muscle were incubated overnight with α-bungarotoxin conjugated with biotinXX (1:80, Invitrogen), anti-phosphorylated NF-H mouse monoclonal antibody (SMI31, 1:100, Covance) and anti-synaptophysin rabbit polyclonal antibody (1:100, Cell Signaling Technologies). After washing, sections were incubated with goat anti-rabbit and anti-mouse IgG conjugated with Alexa 488 (1:1,000 for each, Invitrogen) and streptavidin conjugated with Alexa 564 (1:1,000, Invitrogen) and mounted with Prolong gold (Invitrogen). The stained sections were imaged with an upright microscope (Axio Imager M1, Zeiss). More than 50 NMJs from AR-97Q and heterozygous Hsf-1-knockout AR-97Q mice (13 weeks old) were analysed ($n = 3$).

Quantitative real-time reverse transcriptase PCR (RT-PCR). The mRNA levels of *Hsp70A1* were analysed by real-time RT-PCR as described previously[41]. Detailed methods are described in Supplementary Methods.

Statistical analysis. We analysed the data by using the unpaired Student's *t*-test for two group comparisons, and the Kaplan–Meier and log-rank tests for survival rate using STATVIEW software version 5 (Hulinks, Tokyo, Japan), and denoted *P*-values of 0.05 or less as statistically significant.

References

1. Morimoto, R. I. & Santoro, M. G. Stress-inducible responses and heat shock proteins: new pharmacologic targets for cytoprotection. *Nat. Biotechnol.* **16,** 833–838 (1998).
2. Hartl, F. U., Bracher, A. & Hayer-Hartl, M. Molecular chaperones in protein folding and proteostasis. *Nature* **475,** 324–332 (2011).
3. Wyttenbach, A. Role of heat shock proteins during polyglutamine neurodegeneration: mechanisms and hypothesis. *J. Mol. Neurosci.* **23,** 69–96 (2004).
4. Muchowski, P. J. & Wacker, J. L. Modulation of neurodegeneration by molecular chaperones. *Nat. Rev. Neurosci.* **6,** 11–22 (2005).
5. Hoshino, T. *et al.* Suppression of Alzheimer's disease-related phenotypes by expression of heat shock protein 70 in mice. *J. Neurosci.* **31,** 5225–5234 (2011).
6. Gifondorwa, D. J. *et al.* Exogenous delivery of heat shock protein 70 increases lifespan in a mouse model of amyotrophic lateral sclerosis. *J. Neurosci.* **27,** 13173–13180 (2007).
7. Wacker, J. L. *et al.* Hsp70 and Hsp40 attenuate formation of spherical and annular polyglutamine oligomers by partitioning monomer. *Nat. Struct. Mol. Biol.* **11,** 1215–1222 (2004).
8. Bailey, C. K., Andriola, I. F., Kampinga, H. H. & Merry, D. E. Molecular chaperones enhance the degradation of expanded polyglutamine repeat androgen receptor in a cellular model of spinal and bulbar muscular atrophy. *Hum. Mol. Genet.* **11,** 515–523 (2002).
9. Chan, H. Y. *et al.* Genetic modulation of polyglutamine toxicity by protein conjugation pathways in Drosophila. *Hum. Mol. Genet.* **11,** 2895–2904 (2002).
10. Adachi, H. *et al.* Heat shock protein 70 chaperone overexpression ameliorates phenotypes of the spinal and bulbar muscular atrophy transgenic mouse model by reducing nuclear-localized mutant androgen receptor protein. *J. Neurosci.* **23,** 2203–2211 (2003).
11. Katsuno, M. *et al.* Pharmacological induction of heat-shock proteins alleviates polyglutamine-mediated motor neuron disease. *Proc. Natl Acad. Sci. USA* **102,** 16801–16806 (2005).

12. Anckar, J. & Sistonen, L. Regulation of HSF1 function in the heat stress response: implications in aging and disease. *Ann. Rev. Biochem.* **80,** 1089–1115 (2011).
13. Holmberg, M. *et al.* Spinocerebellar ataxia type 7 (SCA7): a neurodegenerative disorder with neuronal intranuclear inclusions. *Hum. Mol. Genet.* **7,** 913–918 (1998).
14. Yamada, M. *et al.* Polyglutamine disease: recent advances in the neuropathology of dentatorubal-pallidoluysian atrophy. *Neuropathology* **26,** 346–351 (2006).
15. Tanaka, M. *et al.* Intra- and intermolecular beta-pleated sheet formation in glutamine-repeat inserted myoglobin as a model for polyglutamine diseases. *J. Biol. Chem.* **276,** 45470–45475 (2001).
16. Okazawa, H. *et al.* Interaction between mutant ataxin-1 and PQBP-1 affects transcription and cell death. *Neuron* **34,** 701–713 (2002).
17. Subramaniam, S., Sixt, K. M., Barrow, R. & Snyder, S. H. Rhes, a striatal specific protein, mediates mutant-huntingtin cytotoxicity. *Science* **324,** 1327–1330 (2009).
18. Tagawa, K. *et al.* The induction levels of heat shock protein 70 differentiate the vulnerabilities to mutant huntingtin among neuronal subtypes. *J. Neurosci.* **27,** 868–880 (2007).
19. Yamanaka, T. *et al.* Mutant Huntingtin reduces HSP70 expression through the sequestration of NF-Y transcription factor. *EMBO J.* **27,** 827–839 (2008).
20. Adachi, H. *et al.* Widespread nuclear and cytoplasmic accumulation of mutant androgen receptor in SBMA patients. *Brain* **128,** 659–670 (2005).
21. Yamada, M. *et al.* Widespread occurrence of intranuclear atrophin-1 accumulation in the central nervous system neurons of patients with dentatorubral-pallidoluysian atrophy. *Ann. Neurol.* **49,** 14–23 (2001).
22. Nucifora, F. C. *et al.* Interference by huntingtin and atrophin-1 with cbp-mediated transcription leading to cellular toxicity. *Science* **291,** 2423–2428 (2001).
23. Minamiyama, M. *et al.* Sodium butyrate ameliorates phenotypic expression in a transgenic mouse model of spinal and bulbar muscular atrophy. *Hum. Mol. Genet.* **13,** 1183–1192 (2004).
24. Ranganathan, S. *et al.* Mitochondrial abnormalities in spinal and bulbar muscular atrophy. *Hum. Mol. Genet.* **18,** 27–42 (2009).
25. Katsuno, M. *et al.* Testosterone reduction prevents phenotypic expression in a transgenic mouse model of spinal and bulbar muscular atrophy. *Neuron* **35,** 843–854 (2002).
26. Takeyama, K. *et al.* Androgen-dependent neurodegeneration by polyglutamine-expanded human androgen receptor in *Drosophila*. *Neuron* **35,** 855–864 (2002).
27. Katsuno, M. *et al.* Leuprorelin rescues polyglutamine-dependent phenotypes in a transgenic mouse model of spinal and bulbar muscular atrophy. *Nat. Med.* **9,** 768–773 (2003).
28. Chevalier-Larsen, E. S. *et al.* Castration restores function and neurofilament alterations of aged symptomatic males in a transgenic mouse model of spinal and bulbar muscular atrophy. *J. Neurosci.* **24,** 4778–4786 (2004).
29. Kennedy, W. R., Alter, M. & Sung, J. H. Progressive proximal spinal and bulbar muscular atrophy of late onset. A sex-linked recessive trait. *Neurology* **18,** 671–680 (1968).
30. Sobue, G. *et al.* X-linked recessive bulbospinal neuronopathy. A clinicopathological study. *Brain* **112**(Part 1): 209–232 (1989).
31. Orr, H. T. & Zoghbi, H. Y. Trinucleotide repeat disorders. *Ann. Rev. Neurosci.* **30,** 575–621 (2007).
32. Doyu, M. *et al.* Androgen receptor mRNA with increased size of tandem CAG repeat is widely expressed in the neuronal and nonneuronal tissues of X-linked recessive bulbospinal neuronopathy. *J. Neurol. Sci.* **127,** 43–47 (1994).
33. Hayashida, N. *et al.* Heat shock factor 1 ameliorates proteotoxicity in cooperation with the transcription factor NFAT. *EMBO J.* **29,** 3459–3469 (2010).
34. Nagai, Y. *et al.* A toxic monomeric conformer of the polyglutamine protein. *Nat. Struct. Mol. Biol.* **14,** 332–340 (2007).
35. Mason, Jr P. B. & Lis, J. T. Cooperative and competitive protein interactions at the hsp70 promoter. *J. Biol. Chem.* **272,** 33227–33233 (1997).
36. Li, Q. *et al.* Xenopus NF-Y pre-sets chromatin to potentiate p300 and acetylation-responsive transcription from the Xenopus hsp70 promoter *in vivo*. *EMBO J.* **17,** 6300–6315 (1998).
37. Pore, N. *et al.* Sp1 is involved in Akt-mediated induction of VEGF expression through an HIF-1-independent mechanism. *Mol. Biol. Cell* **15,** 4841–4853 (2004).
38. Fujimoto, M. *et al.* Active HSF1 significantly suppresses polyglutamine aggregate formation in cellular and mouse models. *J. Biol. Chem.* **280,** 34908–34916 (2005).
39. Kobayashi, Y. *et al.* Chaperones Hsp70 and Hsp40 suppress aggregate formation and apoptosis in cultured neuronal cells expressing truncated androgen receptor protein with expanded polyglutamine tract. *J. Biol. Chem.* **275,** 8772–8778 (2000).
40. Adachi, H. *et al.* CHIP overexpression reduces mutant androgen receptor protein and ameliorates phenotypes of the spinal and bulbar muscular atrophy transgenic mouse model. *J. Neurosci.* **27,** 5115–5126 (2007).
41. Waza, M. *et al.* 17-AAG, an Hsp90 inhibitor, ameliorates polyglutamine-mediated motor neuron degeneration. *Nat. Med.* **11,** 1088–1095 (2005).
42. La Spada, A. R. *et al.* Androgen receptor gene mutations in X-linked spinal and bulbar muscular atrophy. *Nature* **352,** 77–79 (1991).
43. Nagai, Y., Fujikake, N., Popiel, H. A. & Wada, K. Induction of molecular chaperones as therapeutic strategy for the polyglutamine diseases. *Curr. Pharm. Biotechnol.* **11,** 188–197 (2010).
44. Rimoldi, M., Servadio, A. & Zimarino, V. Analysis of heat shock transcription factor for suppression of polyglutamine toxicity. *Brain Res. Bull.* **56,** 353–362 (2001).
45. Okabe, M. *et al.* 'Green mice' as a source of ubiquitous green cells. *FEBS Lett.* **407,** 313–319 (1997).
46. Mieulet, V. *et al.* S6 kinase inactivation impairs growth and translational target phosphorylation in muscle cells maintaining proper regulation of protein turnover. *Am. J. Physiol. Cell Physiol.* **293,** C712–C722 (2007).
47. Tokui, K. *et al.* 17-DMAG ameliorates polyglutamine-mediated motor neuron degeneration through well-preserved proteasome function in an SBMA model mouse. *Hum. Mol. Genet.* **18,** 898–910 (2009).
48. Marinova, Z. *et al.* Valproic acid induces functional heat-shock protein 70 via Class II histone deacetylase inhibition in cortical neurons: a potential role of Sp1 acetylation. *J. Neurochem.* **111,** 976–987 (2009).
49. Yamanaka, T. *et al.* Mutant huntingtin fragment selectively suppresses Brn-2 POU domain transcription factor to mediate hypothalamic cell dysfunction. *Hum. Mol. Genet.* **19,** 2099–2112 (2010).
50. Hsu, A. L. *et al.* Regulation of aging and age-related disease by DAF-16 and heat shock factor. *Science* **300,** 1142–1145 (2003).
51. Inouye, S. *et al.* Heat shock transcription factor 1 opens chromatin structure of interleukin-6 promoter to facilitate binding of an activator or a repressor. *J. Biol. Chem.* **282,** 33210–33217 (2007).
52. Campeau, E. *et al.* A versatile viral system for expression and depletion of proteins in mammalian cells. *PLoS One* **4,** e6529 (2009).

Acknowledgements

This work was supported by a Global COE Program, MEXT, Japan; MEXT/JSPS KAKENHI Grant Number 21229011, 21689024, 22110005 and 23390230; Health Labour Sciences Research Grants, MHLW, Japan; CREST, JST; and a grant from Kennedy Disease Association.

Author contributions

Project planning was performed by N.K., M.K., A.N. and G.S.; experimental work by N.K., M.K., H.A., M.M., H.D., S.M., Y.M., M.I., G.T., H.N., S.I., Y.F., H.W. and F.T.; data analysis by N.K., M.K. and G.S.; composition of the first draft of the manuscript by N.K. and M.K.; and manuscript layout by A.N. and G.S.

Additional information

Supplementary Information accompanies this paper at http://www.nature.com/naturecommunications

Competing financial interests: The authors declare no competing financial interests.

Reprints and permission information is available online at http://npg.nature.com/reprintsandpermissions/

How to cite this article: Kondo, N. *et al.* Heat shock factor-1 influences pathological lesion distribution of polyglutamine-induced neurodegeneration. *Nat. Commun.* 4:1405 doi: 10.1038/ncomms2417 (2013).

Brain Advance Access published February 28, 2013
doi:10.1093/brain/awt029 Brain 2013: Page 1 of 12 | 1
BRAIN
A JOURNAL OF NEUROLOGY

Loss of TDP-43 causes age-dependent progressive motor neuron degeneration

Yohei Iguchi,[1] Masahisa Katsuno,[1] Jun-ichi Niwa,[2] Shinnosuke Takagi,[1] Shinsuke Ishigaki,[1] Kensuke Ikenaka,[1] Kaori Kawai,[1] Hirohisa Watanabe,[1] Koji Yamanaka,[3,4] Ryosuke Takahashi,[5] Hidemi Misawa,[6] Shoichi Sasaki,[7] Fumiaki Tanaka[1,8] and Gen Sobue[1,4]

1 Department of Neurology, Nagoya University Graduate School of Medicine, Nagoya 466-8550, Japan
2 Stroke Centre, Aichi Medical University, Aichi 480-1195, Japan
3 Laboratory for Motor Neuron Disease, RIKEN Brain Science Institute, Wako, Saitama 351-0198, Japan
4 CREST, Japan Science and Technology Agency, 4-1-8, Honcho, Kawaguchi, Saitama 332-0012, Japan
5 Department of Neurology, Kyoto University Graduate School of Medicine, Kyoto 606-8507, Japan
6 Department of Pharmacology, Keio University Faculty of Pharmacy, Tokyo 105-8512, Japan
7 Department of Neurology, Neurological Institute, Tokyo Women's Medical University, Tokyo 162-8666, Japan
8 Department of Neurology and Stroke Medicine, Yokohama City University Graduate School of Medicine, Yokohama 236-0004, Japan

Correspondence to: Gen Sobue
Showa-ku, Nagoya 466-8550,
Japan
E-mail: sobueg@med.nagoya-u.ac.jp

Amyotrophic lateral sclerosis is a devastating, progressive neurodegenerative disease that affects upper and lower motor neurons. Although several genes are identified as the cause of familial cases, the pathogeneses of sporadic forms, which account for 90% of amyotrophic lateral sclerosis, have not been elucidated. Transactive response DNA-binding protein 43 a nuclear protein regulating RNA processing, redistributes to the cytoplasm and forms aggregates, which are the histopathological hallmark of sporadic amyotrophic lateral sclerosis, in affected motor neurons, suggesting that loss-of-function of transactive response DNA-binding protein 43 is one of the causes of the neurodegeneration. To test this hypothesis, we assessed the effects of knockout of transactive response DNA-binding protein 43 in mouse postnatal motor neurons using Cre/loxp system. These mice developed progressive weight loss and motor impairment around the age of 60 weeks, and exhibited degeneration of large motor axon, grouped atrophy of the skeletal muscle, and denervation in the neuromuscular junction. The spinal motor neurons lacking transactive response DNA-binding protein 43 were not affected for 1 year, but exhibited atrophy at the age of 100 weeks; whereas, extraocular motor neurons, that are essentially resistant in amyotrophic lateral sclerosis, remained preserved even at the age of 100 weeks. Additionally, ultra structural analysis revealed autolysosomes and autophagosomes in the cell bodies and axons of motor neurons of the 100-week-old knockout mice. In summary, the mice in which transactive response DNA-binding protein 43 was knocked-out specifically in postnatal motor neurons exhibited an age-dependent progressive motor dysfunction accompanied by neuropathological alterations, which are common to sporadic amyotrophic lateral sclerosis. These findings suggest that transactive response DNA-binding protein 43 plays an essential role in the long term maintenance of motor neurons and that loss-of-function of this protein seems to contribute to the pathogenesis of amyotrophic lateral sclerosis.

Keywords: transactive response DNA-binding protein 43; amyotrophic lateral sclerosis; axonal degeneration; autophagosome

Abbreviations: ALS = amyotrophic lateral sclerosis; FTLD = frontotemporal lobar degeneration; TDP CKO = motor neuron-specific TDP-43 knockout; TDP hCKO = TDP heterozygous CKO

Received July 20, 2012. Revised December 17, 2012. Accepted December 28, 2012.

Introduction

Amyotrophic lateral sclerosis (ALS) is a progressive, fatal neurodegenerative disease that affects upper and lower motor neurons in the brain stem and spinal cord. Although previous studies using animal models of ALS have focused mainly on the toxicity of mutant SOD1, one of the causative genes of familial ALS (ALS1), there are pathophysiological differences between ALS1 and sporadic ALS that accounts for ~90% of ALS. The most striking recent discovery regarding ALS is that transactive response DNA-binding protein 43 (TDP-43) was identified as a major component of ubiquitinated neuronal cytoplasmic inclusions in both sporadic ALS and frontotemporal lobar degeneration (FTLD) (Arai *et al.*, 2006; Neumann *et al.*, 2006). In addition, TDP-43 is a causative gene of familial ALS (ALS10) (Gitcho *et al.*, 2008; Kabashi *et al.*, 2008; Sreedharan *et al.*, 2008; Yokoseki *et al.*, 2008). Taken together, these data suggest that TDP-43 plays a key role in the pathogenesis of sporadic ALS. Although TDP-43 is a nuclear protein, it redistributes to the cytoplasm and forms aggregates in affected neurons of patients with sporadic ALS (Arai *et al.*, 2006; Neumann *et al.*, 2006), suggesting that loss of TDP-43 function underlies sporadic ALS pathogenesis. TDP-43 is known to regulate gene transcription, stability of messenger RNA, and exon splicing through interactions with RNA, heterogeneous nuclear ribonucleoproteins and nuclear bodies (Wang *et al.*, 2004; Ayala *et al.*, 2005; Buratti *et al.*, 2005, 2010; Strong *et al.*, 2007; Polymenidou *et al.*; 2011; Sephton *et al.*, 2011; Tollervey *et al.*, 2011). Knockdown of TDP-43 in neuronal cells inhibits neurite outgrowth and diminishes cell viability (Iguchi *et al.*, 2009), whereas TDP-43 depletion induces apoptosis in HeLa or U2OS cells (Ayala *et al.*, 2008). In addition, *Drosophila* without TDP-43 present deficient locomotive behaviours, reduced life span and anatomical defects at neuromuscular junctions (Feiguin *et al.*, 2009). TDP-43-depleted zebrafish exhibit swimming deficits along with excessive, premature branching and shortened motor axons (Kabashi *et al.*, 2011). Furthermore, TDP-43 knockout mice are embryonic lethal (Kraemer *et al.*, 2010; Sephton *et al.*, 2010; Wu *et al.*, 2010), and postnatal deletion of TDP-43 leads to rapid death with loss of body fat (Chiang *et al.*, 2010). Although these findings indicate that TDP-43 is essential for survival of mice at both embryonic and post-natal stages, the effects of TDP-43 depletion in postnatal mammalian neurons have not been fully elucidated. In the present study, we generated motor neuron-specific TDP-43 knockout (TDP CKO) mice using the Cre/loxP recombination system to investigate the effects of TDP-43 loss on postnatal motor neurons in mice.

Materials and methods

Generation and maintenance of TDP-43 conditional knockout mouse

The targeting construct was designed to insert an Frt-flanked neomycin cassette and a loxP site upstream, and a loxP site downstream of the second exon of the *Tardbp* gene. This construct was electroporated into iTL1 BA1 (C57BL/6 × 129/SvEv) hybrid embryonic stem cells. Correctly targeted embryonic stem cells were injected into recipient blastocysts and chimeric mice were bred with C57BL/6J mice. The resulting En1flox-neo mice were then bred to C57BL/6J mice constitutively expressing Flp recombinase to remove the Frt-flanked neo cassette, generating En1flox offspring. En1flox mutant mice were backcrossed with C57BL/6J mice for at least five generations, and then crossed with VAChT-Cre.Fast mice, which are the most validated mice that specifically express Cre in motor neurons (Misawa *et al.*, 2003). To generate TDP-43 conditional knockout mice, we crossed TDP-43$^{flox/flox}$ mice with TDP-43$^{flox/+}$/VAChT-Cre mice. Finally, we obtained TDP-43$^{flox/flox}$/VAChT-Cre (motor neuron-specific TDP-43 knockout: TDP CKO), TDP-43$^{flox/+}$/VAChT-Cre (TDP heterozygous CKO: TDP hCKO), TDP-43$^{flox/flox}$ and TDP-43$^{flox/+}$ mice. The TDP-43$^{flox/flox}$ mice were then used as control littermates in the present analyses. Mice were kept on a 12-h light/12-h dark cycle, with food and water provided *ad libitum*. All animal experiments were performed in accordance with the National Institutes of Health Guide for the Care and Use of Laboratory Animals and under the approval of the Nagoya University Animal Experiment Committee (Nagoya, Japan).

Neurological and behavioural testing

The control ($n = 21$) and TDP CKO ($n = 20$) mice were subjected to the Rotarod task (Economex Rotarod; Columbus Instruments) weekly as described previously (Katsuno *et al.*, 2002). Grip strength was measured weekly by a grip strength meter (MK-380M, Muromachi kikai Co. LTD). During this test, the mice griped the mesh with four limbs and their tail was pulled backwards. Gait stride was measured from 50 cm of footsteps, and the average value was recorded for each mouse.

Immunofluorescent analysis and immunohistochemistry

For immunofluorescent analysis, we perfused 20 ml of a 4% paraformaldehyde fixative in phosphate buffer (WAKO Corp.) through the left cardiac ventricle of mice deeply anaesthetized with medetomidine (0.3 mg/kg), midazolam (4 mg/kg) and butorphanol (5 mg/kg), interperitoneally. Tissues postfixed overnight in 10% phosphate-buffered formalin were then processed for paraffin embedding. We then deparaffinized 3 -μm thick tissue sections and dehydrated them with alcohol. Sections were first microwaved for 20 min in 50 mM citrate buffer (pH 6.0), treated with TNB blocking buffer (PerkinElmer) and incubated overnight with anti-TDP-43 rabbit polyclonal antibody (1:1000, ProteinTech), anti-choline-acetyltransferase (ChAT) goat polyclonal antibody (1:100, Milipore), anti-microtubule-associated protein 1 light chain 3 (LC3) mouse monoclonal antibody (1:1000, MBL), phosphorylated neurofilament-H (pNF-H) mouse monoclonal antibody (SMI31) (1:1000, Covance), or anti-neuronal nuclei (NeuN) mouse monoclonal antibody (1:100, Millipore). After washing, for the ChAT staining, sections were incubated with biotinylated donkey anti-goat IgG (1:300, Vector Lab.) for 30 min, washed and incubated with streptavidin conjugated with Alexa Fluor® 546 (1:1000, Invitrogen) for 30 min. For the other antigens, sections were incubated with the indicated secondary antibody and TO-PRO®3 (Invitrogen), a nuclear marker, for 30 min, mounted with ProLong® Gold Antifade reagent (Invitrogen), and then imaged with a laser confocal microscope (LSM710, Carl Zeiss). For immunohistochemistry, sections were incubated overnight with anti-glial fibrillary acidic protein (GFAP) mouse

monoclonal antibody (1:1000, Sigma-Aldrich), stained using the DAKO EnVision™+ HRP system (Dako Corp.) and photographed with an optical microscope (Axio Imager M1). The immunoreactive area in the ventral horn of TDP CKO mice and control littermates at the indicated ages ($n = 3$ for each age) was analysed with WinROOF (Mitani). The binary treatment included application of a staining intensity threshold and size exclusion criteria to distinguish the significant structures from the background signals. All sections analysed were treated with the same threshold and exclusion criteria.

Retrograde FluoroGold neurotracer labelling

Retrograde labelling of motor neurons was performed as described previously (Katsuno *et al.*, 2006). Briefly, a total volume of 4.5 µl of 2.5% FluoroGold solution (Biotium) was injected into the gastrocnemius muscle of anaesthetized mice. Lumbar spinal cords were removed 46 h after FluoroGold administration. The frozen optimal cutting temperature (OCT) compound-embedded samples were sectioned longitudinally on a cryostat at 10 µm and mounted on silane-coated slides. After the FluoroGold labelled motor neurons in the L5 segment was photographed with Zeiss Axio Imager M1 (Carl Zeiss), the sections were fixed with 4% paraformaldehyde, stained with anti-TDP-43 and anti-ChAT antibody, and photographed with LSM710. For the quantification of retrograde labelling, we measured every third section (a total of five sections in L5 ventral horn), and counted the degree of FluoroGold labelling in motor neurons of two control mice, and TDP-43-positive or -negative motor neurons of two TDP CKO mice.

Electron microscopy

Under the deep anaesthesia, 2-year-old TDP CKO mice and control littermates were transcardially perfused with 3% paraformaldehyde and 1% glutaraldehyde in PBS. The spinal cords and sciatic nerves were removed, and postfixed overnight in the perfusing solution. After fixation, the spinal cords were immersed in the solution (0.1 M cacodylic acid, 2% paraformaldehyde, 2.5% glutaraldehyde) for 12 h. The anterior half of lumbar spinal cord was sectioned transversely, postfixed in 1% osmium tetroxide for several hours, dehydrated and embedded in epoxy resin. Each block was cut into serial semithin sections (~1-µm thick). These sections were stained with toluidine blue. Appropriate portions of the sections were cut into ultrathin sections, which were then stained with uranyl acetate and lead citrate. Two-year-old TDP CKO mice and control littermates were analysed. Electron microscopic photographs were obtained under an original magnification of ×5000 and printed at a final magnification of ×9500.

Analysis of muscle, neuromuscular junction and motor axon

To investigate the presence of muscle atrophy, gastrocnemius muscles were dissected free, quickly frozen by immersion in cooled acetone and powdered CO_2. Ten-micrometre thick transverse frozen sections were stained with haematoxylin and eosin. For analysis of neuromuscular junctions, 30-µm thick frozen longitudinal sections of the tibialis anterior muscle were incubated overnight with alpha bungarotoxin conjugated with biotin-XX (1:80, Invitrogen), anti-pNF-H mouse monoclonal antibody (SMI31, 1:100) and anti-synaptophysin rabbit polyclonal antibody (1:100, Cell Signaling Technologies). After washing, sections were incubated with goat anti-rabbit and anti-mouse IgG conjugated with Alexa Fluor® 488 (1:1000 for each, Invitrogen) and streptavidin conjugated with Alexa Fluor® 564 (1:1000, Invitrogen) and mounted with ProLong® gold (Invitrogen). The stained sections were imaged with a laser scanning confocal microscope (LSM710, Carl Zeiss). More than 100 neuromuscular junctions from TDP CKO mice aged 20, 50, 80 and 100 weeks were analysed ($n = 3$ mice for each group). For morphological analyses, epoxy resin embedded transverse sections of L5 ventral roots were stained with toluidine blue. L5 ventral roots of 20, 50 and 100 week-old mice ($n = 6$ axons for each group) were assessed. The diameter of myelinated fibres was automatically measured using a computer-assisted image analyser (Luzex FS), as described previously (Katsuno *et al.*, 2002). Paraffin embedded transverse sections of L4 ventral roots of 100-week-old mice were stained with an antibody against ChAT and photographed by Zeiss Axio Imager M1.

Quantification and morphological analysis of motor neurons

For the quantifications and morphological analyses of motor neurons, we performed the immunofluorescent analyses of the paraffin-embedded sections stained with anti-TDP-43 and anti-ChAT antibodies of L5 spinal cord ($n = 5$ for each) and brain stem ($n = 3$ for each) of control and TDP CKO mice. All the neurons within the every fifth sections from the 50 consecutive sections of lumbar spinal cord, or every third sections from all consecutive sections of brain stem including the each cranial motor nucleus were assessed using AxioVision softwear (Carl Zeiss), after samples were photographed by Zeiss Axio Imager M1 (Carl Zeiss). The ChAT-positive neurons in the ventral horns or cranial nuclei were regarded as motor neurons. We examined the presence of nuclear immunoreactivity for TDP-43 in ventral horns and brainstems, and calculated the TDP-43-knockout efficiencies, the number of remaining motor neurons, and the size of motor neurons in each group. To evaluate the involvement of gamma-motor neuron, we measured the number of large ($>250\,\mu m^2$) or small ($<250\,\mu m^2$) lumbar motor neurons.

Statistical analyses

Statistical differences were analysed by Kaplan–Meier and logrank test for survival rate, ANOVA and Bonferroni *post hoc* analyses for multiple group comparisons and the unpaired Student's *t*-test for two group comparisons (SPSS version 15.0, SPSS Inc.).

Results

Generation of TDP CKO mice

We constructed a TDP-43flox allele by flanking the second exon of the mouse TDP-43 gene (*Tardbp*) with loxP sites (Supplementary Fig. 1A and B). Because the second exon contains the *Tardbp* start codon, Cre-mediated deletion of this exon inhibits mouse TDP-43 translation. To delete TDP-43 expression specifically in motor neurons, TDP-$43^{flox/flox}$ mice were crossed with VAChT-Cre.Fast mice, in which Cre expression is mostly restricted in the postnatal somatomotor neurons (Misawa *et al.*, 2003). The immunofluorescent analysis of the ventral horn from TDP CKO mice at post-natal Day 2 showed that all the assessed motor neurons were positive for TDP-43 (Supplementary Fig. 1C). On

the other hand, the quantitative analysis of the lumbar ventral horn and hypoglossal nucleus from 10-week-old TDP CKO mice showed that TDP-43 was knocked-out in 48% of motor neurons in the lumbar ventral horn and 45% in the hypoglossal nucleus (Fig. 1A and B). In addition, reverse transcriptase PCR analysis of total RNA from motor neurons isolated by laser microdissection, revealed that exon 2 of *Tarbdp* was partially skipped under the Cre expression (Supplementary Fig. 1D and E). Immunoblot analysis showed that the TDP-43 protein expressions in liver, kidney, heart, skeletal muscle and cerebral cortex of TDP CKO mice were not altered compared with their control littermates (Supplementary Fig. 1F). Immunofluorescent analysis of the

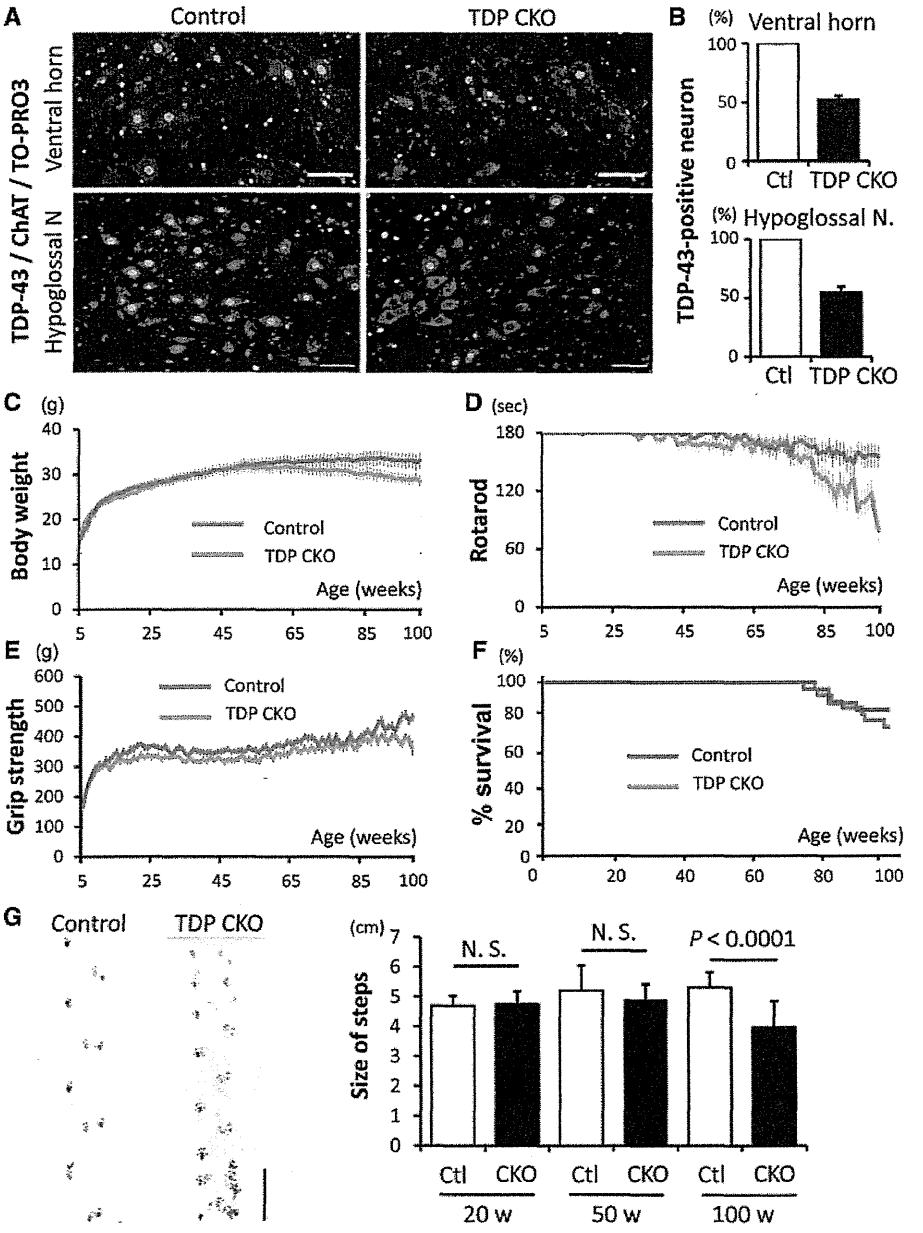

Figure 1 Progressive motor dysfunction in TDP CKO mice. (**A**) Immunofluorescent stainings (TDP-43; green, ChAT; red, TO-PRO3; blue) of lumbar ventral horn and hypoglossal nucleus of 10-week-old control and TDP CKO mice. (**B**) Percentage of TDP-43-positive motor neurons in the lumbar ventral horn and hypoglossal nucleus (N.) of 10-week-old control (Ctl) and TDP CKO mice ($n = 3$ for each group). (**C–E**) Body weight (**C**), Rotarod task (**D**), and grip strength (**E**) phenotypes of control (red line, $n = 21$) and TDP CKO mice (blue line, $n = 20$). Error bars indicate SEM. (**F**) Survival rates of control ($n = 27$) and TDP CKO mice ($n = 26$). (**G**) The average length of hindpaw steps in 20-week-old ($n = 6$ for each), 50-week-old ($n = 6$ for each), and 100-week-old ($n = 15$ for each) control and TDP CKO mice. Error bars indicate SD. Scale bars: **A** = 50 μm; **G** = 5 cm. N.S. = not significant.

lumbar dorsal horn of 10-week-old control, TDP CKO and TDP hCKO mouse showed that all the assessed neurons were positive for TDP-43 (Supplementary Fig. 2). In addition, the analyses of 100-week-old control, TDP CKO and TDP hCKO mice demonstrated that TDP-43 was not excised in the neurons of the primary motor cortex, putamen, deep cerebellar nucleus and cerebellar cortex of TDP CKO or TDP hCKO mouse (Supplementary Figs 3 and 4).

TDP-43 CKO mice develop progressive motor dysfunction

The earliest symptom of motor deficit in TDP CKO mice was tremor, which appeared as early as 50 weeks. TDP CKO mice exhibited progressive weight loss beginning ~60 weeks (Fig. 1C), when muscle atrophy of the trunk and hind limb was detectable. The grip strength and motor performances in the Rotarod task of TDP CKO mice were lower than their control littermates (Fig. 1D and E) beginning at 85 and 75 weeks, respectively. At 100 weeks, TDP CKO mice were significantly different from the control littermates in body weight ($P = 0.04$), rotarod ($P = 0.001$) and grip strength ($P = 0.002$). The average length of hindpaw steps of TDP CKO mice was significantly shorter than that of control littermates in 100 weeks of age ($P = 0.000001$; Fig. 1G). The survival rate of TDP CKO mice, however, was not altered compared with that of control littermates (Fig. 1F). Analyses of TDP-43$^{flox/+}$ and TDP-43$^{flox/+}$/VAChT-Cre (TDP hCKO) mice, which resulted in heterozygous loss of TDP-43 in motor neurons, showed that body weight, Rotarod task, grip strength and length of hindpaw steps were not significantly different between the two transgenic groups (Supplementary Fig. 5A–D).

TDP-43 depletion leads to atrophy of spinal motor neurons

Because TDP CKO mice exhibited progressive motor impairment, we focused on the morphology of spinal motor neurons. The immunofluorescent analysis of the lumbar ventral horn in 100-week-old TDP CKO mice revealed that motor neurons without TDP-43 were significantly smaller than those with TDP-43 and those in control littermates (Fig. 2A–C). Although TDP-43 was knocked-out in 49% of motor neurons in TDP CKO mice, the number of motor neurons in TDP CKO mice did not differ from that in control littermates (Fig. 2D and E). A time course analysis of TDP-43-lacking motor neurons in TDP CKO mice showed that neuronal atrophy was evident at 100 weeks (Fig. 2F). In addition, we measured TDP-43 knockout efficiency in the small (>250 μm^2) and large (<250 μm^2) lumbar motor neurons. The results showed that there was no difference in the knockout efficiency between the small and large motor neurons (Supplementary Fig. 6A), suggesting that the TDP-43-knockout efficiency in the gamma-motor neurons of TDP CKO mice is similar to that of alpha-motor neurons. The measurement of the average motor neuron number showed that the number of TDP-43-lacking large motor neurons decreased at 100 weeks of age compared with TDP-43-positive motor neurons, whereas the number of TDP-lacking small motor neurons increased, indicating that postnatal deletion of TDP-43 leads to atrophy of the alpha-motor neurons in the aged TDP CKO mice (Supplementary Fig. 6B). This view is supported

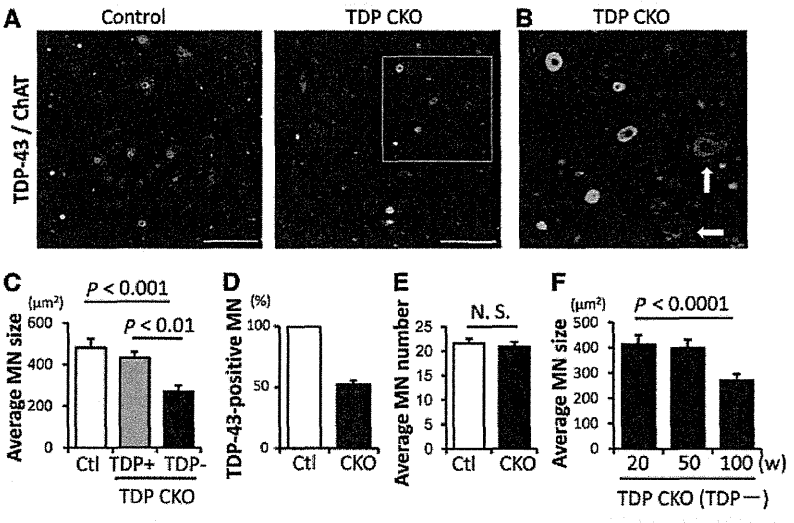

Figure 2 Morphological analysis of spinal motor neurons. (**A** and **B**) Immunofluorescent stainings (TDP-43, green; ChAT, red) of lumbar ventral horn from 100-week-old control (Ctl) and TDP CKO mice. (**B**) Enlarged image of the area marked in **A** (*left*). TDP-43-lacking motor neurons (arrows) were significantly smaller than TDP-43-positive motor neurons. (**C**) Percentage of TDP-43-positive motor neurons in the lumbar ventral horn of 100-week-old mice ($n = 5$ for each group). (**D**) Average size of spinal motor neurons (MN) in 100-week-old mice ($n = 5$ for each group). Error bars indicate SD. (**E**) Average number of spinal motor neurons in 100-week-old mice ($n = 5$ for each group). Error bars indicate SD. (**F**) Time course of atrophy of TDP-43-lacking motor neurons ($n = 5$ for each age). TDP+ = TDP-43-positive neurons; TDP− = TDP-43-negative neurons. Scale bars = 100 μm.

by the immunofluorescent analysis of the lumbar ventral horn from 100-week-old TDP CKO mice showing that the TDP-43-lacking alpha-motor neuron, which was positive for NeuN and ChAT, was smaller than the TDP-43-positive alpha-motor neuron (Supplementary Fig. 6C). On the other hand, there was no morphological difference in the motor neurons between TDP hCKO and TDP-43$^{flox/+}$ mice (Supplementary Fig. 5E).

TDP-43 depletion affects motor axon, neuromuscular junction and skeletal muscle

The toluidine blue staining of transverse sections of L5 ventral root exhibited axonal degeneration in a subset of large myelinated fibres of TDP CKO mice from 50 weeks (Fig. 3A). Quantitative analyses of the ventral roots demonstrated the decrease of large myelinated fibres and increase of small myelinated fibres in 100 week-old TDP CKO mice (Fig. 3A). The immunofluorescent analysis using anti-ChAT antibody also exhibited the loss of large motor axons in the ventral root of TDP CKO mice (Fig. 3B). Axial sections of the gastrocnemius muscle in 100-week-old TDP CKO mice exhibited grouped atrophy, a neurogenic muscular change (Fig. 3C). Whereas all assessed neuromuscular junctions in the control littermates were innervated, in the TDP CKO mice, the percentage of denervated neuromuscular junctions increased progressively after the age of 50 weeks, concomitant with motor impairment and motor neuron atrophy (Fig. 3D). In analyses of retrograde FluoroGold labelling of the motor neurons in TDP CKO mice, the degree of labelling was significantly less in the TDP-43-lacking motor neurons than in the TDP-43-positive motor neurons (Fig. 3E).

Assessment in motor nuclei of cranial nerves

The histopathology of patients with ALS is characterized by the selective loss of motor neurons with scarcely detectable damage in the extraocular motor nuclei. To examine the region-specific neuropathology in TDP CKO mice, we quantitatively analysed the motor nuclei of cranial nerves. In the trigeminal motor, facial, hypoglossal and abductor nuclei of 100-week-old TDP CKO mice, ~50% of motor neurons were negative for TDP-43, but in the oculomotor nucleus, the efficiency of TDP-43 depletion was only ~25% (Supplementary Fig. 7). Morphological analysis of the trigeminal motor, facial and hypoglossal nuclei in 100-week-old TDP CKO mice revealed that TDP-43-lacking motor neurons were significantly smaller than those with TDP-43 or those of the control littermates (Fig. 4A–C), whereas those in the oculomotor and the abductor nuclei were preserved (Fig. 4D and E), suggesting that this mouse model recapitulates the selective vulnerability of motor neuron in ALS. The time course analysis of the hypoglossal motor nucleus showed that the atrophy of the motor neuron was evident from 50 weeks. The number of motor neurons in these nuclei of TDP CKO mice was not altered compared with the control littermates, as was shown in the spinal cord (Fig. 4A–E).

Astrogliosis in ventral horn and accumulation of phosphorylated neurofilament in motor neurons of TDP CKO mice

Immunohistochemistry of the ventral horn showed that the number of astrocytes progressively increased in TDP CKO mice (Fig. 5A). Phosphorylated neurofilament accumulated in the cytoplasm of TDP-43-lacking motor neurons of TDP CKO mice, but not in motor neurons with TDP-43 in TDP CKO mice or those of control littermates (Fig. 5B).

Formation of autophagosomes in motor neurons of TDP CKO mice

Recent studies indicate that autophagosomes accumulate in motor neurons of patients with sporadic ALS and animal models of motor neuron diseases (Li *et al.*, 2008; Sasaki, 2011; Tian *et al.*, 2011). Therefore, we investigated autophagy-related pathology in 100-week-old control and TDP CKO mice. The immunofluorescent analysis showed LC3-positive puncta in 37% of TDP-43-lacking motor neurons, but not in TDP-43-positive motor neurons in TDP CKO mice or those of the control littermates (Fig. 6A). TDP-43-lacking motor neurons with the puncta were significantly smaller than those without the puncta (Fig. 6B). The ultrastructure of motor neurons from 100-week-old TDP CKO mice demonstrated that autophagy-related structures such as autolysosomes and autophagosomes were accumulated in the cell bodies of motor neurons (Fig. 6C–E), proximal motor axon (Fig. 6F), and sciatic nerve of TDP CKO mice (Fig. 6G–H). These structures were not seen in the control mice as far as we observed.

Discussion

Although TDP-43 is an established pathological hallmark of ALS, it remains unclear how TDP-43 contributes to the pathogenesis. In the present study, we showed that TDP CKO mice, in which TDP-43 was knocked-out specifically in postnatal motor neurons, developed an age-dependent progressive motor impairment such as gait disturbance and muscle atrophy, suggesting that the loss-of-function of TDP-43 in postnatal motor neurons plays a causative role in the neurodegenerative process of ALS. There has been a great deal of debate about whether loss or gain of TDP-43 function causes the neurodegeneration (Lee *et al.*, 2011). Several mouse, rat and primate models overexpressing wild-type or disease mutant TDP-43 recapitulate the phenotype of ALS or FTLD (Wegorzewska *et al.*, 2009; Shan *et al.*, 2010; Stallings *et al.*, 2010; Tsai *et al.*, 2010; Wils *et al.*, 2010; Xu *et al.*, 2010; Zhou *et al.*, 2010; Igaz *et al.*, 2011; Swarup *et al.*, 2011; Uchida *et al.*, 2012); however, redistributions and cytoplasmic inclusions of TDP-43 are generally rare and several models exhibit cytoplasmic mitochondrial aggregation, which is not common in ALS. The expression of endogenous TDP-43 is suppressed in neurons expressing human TDP-43-delta nuclear localization signal as well as those expressing human wild-type TDP-43, suggesting that

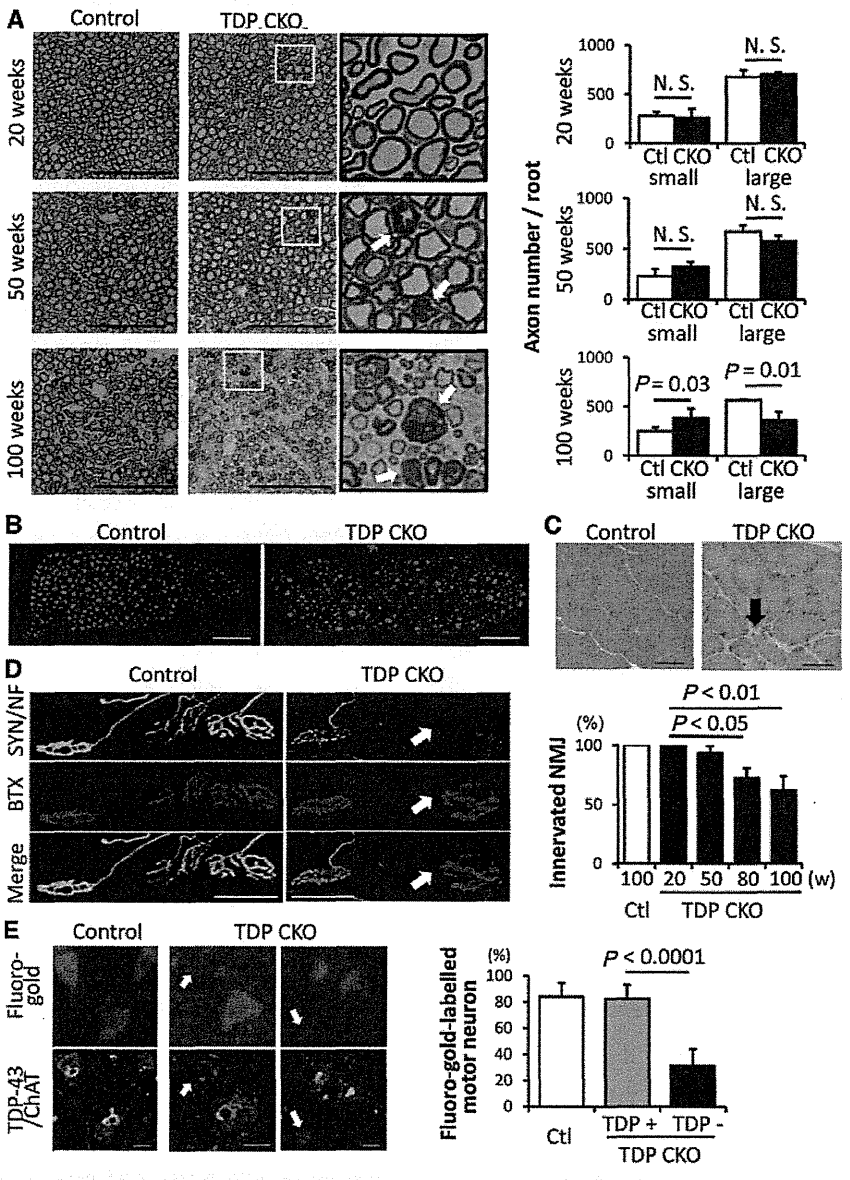

Figure 3 Analysis of motor axons, neuromuscular junctions, and skeletal muscles. (**A**) Toluidine blue staining images and the number of small myelinated fibres (<5 μm) and large myelinated fibres (>5 μm) in the L5 ventral root from 20, 50 and 100-week-old control and TDP CKO mice (n = 6 axons of each). The enlarged image of the yellow-framed area is also shown. Arrows indicate axonal degenerations. Scale bars = 100 μm. Error bars indicate SD. (**B**) Immunofluorescent staining of the L4 ventral root in 100-week-old mice with an anti-ChAT antibody. (**C**) Haematoxylin and eosin staining of gastrocnemius muscles of 100-week-old mice. Axial sections from TDP CKO mice exhibited grouped atrophy (arrow), whereas the control littermates showed no such phenomenon. (**D**) Immunofluorescent staining [synaptophysin (SYN) and phospho-neurofilament (NF), green; bungarotoxin (BTX), red] of neuromuscular junctions (NMJ) in 100-week-old mice and a time course analysis of neuromuscular junctions in TDP CKO mice. Denervated neuromuscular junctions (arrow) are indicated by the lack of synaptophysin and phospho-neurofilament staining. Scale bars = 50 μm. Error bars indicate SD (n = 3). (**E**) FluoroGold labelling (blue) and immunofluorescence staining (TDP-43, green; ChAT, red) of lumbar motor neurons. Retrograde FluoroGold labelling was significantly attenuated in TDP-43-lacking motor neurons but not in TDP-43-positive neurons in 100-week-old TDP CKO mice (arrows). Scale bars = 20 μm. Error bars indicate SD (n = 10).

mutant TDP-43 may cause neurodegeneration through inhibition of normal TDP-43 function (Igaz *et al.*, 2011). On the other hand, TDP-43 knockout mice result in embryonic lethal phenotypes (Kraemer *et al.*, 2010; Sephton *et al.*, 2010; Wu *et al.*, 2010), and systemic postnatal deletion of this molecule led to rapid death (Chiang *et al.*, 2010). Although TDP-43-depleted models of *Drosophila* and zebrafish exhibit neurodevelopmental deficits in motor axons (Feiguin *et al.*, 2009; Kabashi *et al.*, 2011), the

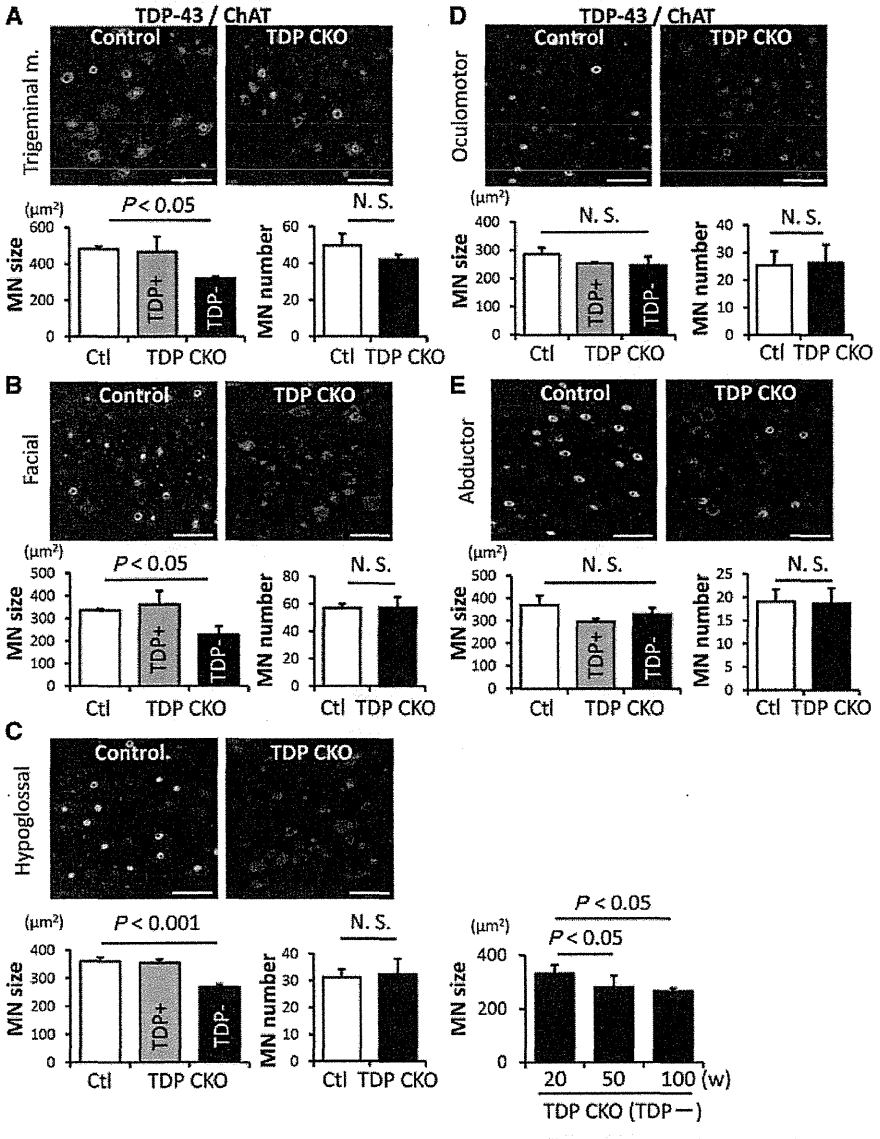

Figure 4 Morphological analysis of cranial motor nuclei. (**A–E**) Immunofluorescent analysis (TDP-43, green; ChAT, red) of motor neurons in the trigeminal motor (m.) (**A**), facial (**B**), hypoglossal (**C**), oculomotor (**D**), and abductor (**E**) nuclei from 100-week-old control ($n = 3$) and TDP CKO mice ($n = 3$). Graphs show the average size and number of motor neurons in each area. TDP+ = TDP-43-positive neuron; TDP− = TDP-43-negative neuron. Error bars indicate SD. Scale bars = 50 μm. MN = motor neuron; N.S. = not significant.

role of TDP-43 in postnatal mammalian neurons has not been fully elucidated. In the present study, we clarified that TDP CKO mice, in which TDP-43 was specifically knocked-out by Cre recombinase in postnatal motor neurons, develops a progressive motor neuronal degeneration as seen in ALS, suggesting that TDP-43 is essential for the long term maintenance of postnatal motor neurons in mice. Although TDP CKO mice developed ALS-like motor impairment, the mortality of the mice was not different from that of control littermates. This might be due to the knockout efficiency of TDP-43, which occurred in ~50% of motor neurons, or due to the life span of mice, which is considerably shorter than the disease duration of patients with ALS. Moreover, there were no significant alterations in body weight, motor function or morphology of motor neurons in our TDP heterozygous CKO (TDP hCKO) mice. Because previous studies demonstrated that the protein expression of TDP-43 was not reduced in various tissues of heterozygous TDP-43 knockout mice (Kraemer *et al.*, 2010; Sephton *et al.*, 2010; Wu *et al.*, 2010), TDP-43 depletion is likely insufficient to affect the motor neurons in our TDP hCKO mice. At the same time, these data suggest that expression of Cre itself did not affect the vulnerability of the mouse motor neurons over 2 years.

An earlier study demonstrates that the motor neuron-specific TDP-43 knockout mouse carrying HB9-Cre exhibits early-onset

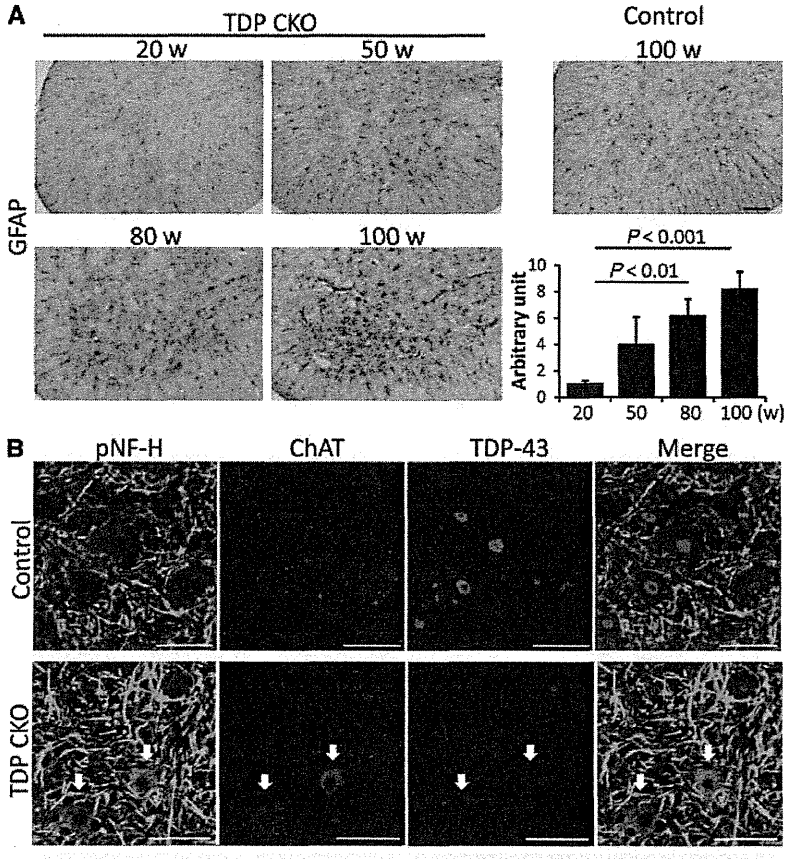

Figure 5 Astrogliosis and neuronal accumulation of phosphorylated neurofilament. (**A**) Immunohistochemistry against GFAP in the ventral horn and a time course analysis of astrogliosis. Error bars indicate SD ($n = 3$ for each age). (**B**) Immunofluorescent staining against pNF-H (green), ChAT (red) and TDP-43 (blue). pNF-H was accumulated in the cell bodies of TDP-43-lacking motor neurons of TDP CKO mice (arrows). Scale bars: **A** = 100 μm; **B** = 50 μm.

motor dysfunction and develops motor neuronal loss earlier than 10 weeks of age (Wu *et al.*, 2012). However, given that the Cre-mediated recombination using the *HB9* promoter began at the developmental stage E9.5 (Arber *et al.*, 1999), this model possibly reflects the loss-of-function of TDP-43 in the motor neuron development. By contrast, because the Cre expression in VAChT-Cre.Fast mice is mediated by the VAChT promoter, the number of Cre-expressing motor neurons in VAChT-Cre.Fast mice is scarcely detected at prenatal stages, but becomes maximum in number at 5 weeks (Misawa *et al.*, 2003). We also confirmed that TDP-43 was not excised in spinal motor neurons of TDP CKO mice at post-natal Day 2, but knocked-out in ~50 % of motor neurons of the 10-week-old mice. This temporal pattern of Cre expression appears to contribute to the late-onset progressive motor dysfunction in our TDP CKO mice and enable the assessment of loss of TDP-43 functions in mouse motor neurons at the postnatal stage. As far as we investigated, TDP-43 was knocked-out in spinal motor neurons beginning at 10 weeks, but the function and morphology of motor neurons were unexpectedly preserved for 1 year in TDP CKO mice, suggesting that the loss of TDP-43 was compensated in motor neurons of young mice, but triggered neuronal vulnerability with the ageing process. Given that ALS is an age-related neurodegenerative disease and that the disease develops after middle age even in inherited cases with TDP-43 mutations (Gitcho *et al.*, 2008; Kabashi *et al.*, 2008; Sreedharan *et al.*, 2008; Yokoseki *et al.*, 2008), our TDP CKO mice appear to be a model that recapitulates the age-dependent phenotypes of ALS. However, as TDP CKO mice lack some aspects of human ALS pathology, such as cytoplasmic inclusions of TDP-43 and the involvement of upper motor neurons, the use of this model for therapeutic research needs further validation.

In the histopathological analyses, TDP CKO mice exhibited the atrophy of motor neurons, degeneration of large motor axons, denervation of neuromuscular junctions and grouped atrophy of skeletal muscles, all of which are common to the pathology of human motor neuron disease. The disruption of retrograde labelling in TDP-43-lacking motor neurons suggests that TDP-43 depletion directly induces neuronal dysfunction. Interestingly, the axonal degenerations were evident in the ventral root of TDP CKO mice at 50 weeks of age, when the morphology of lumbar motor neurons was not altered. These findings are compatible with the fact that ALS pathology initially manifests at the axon

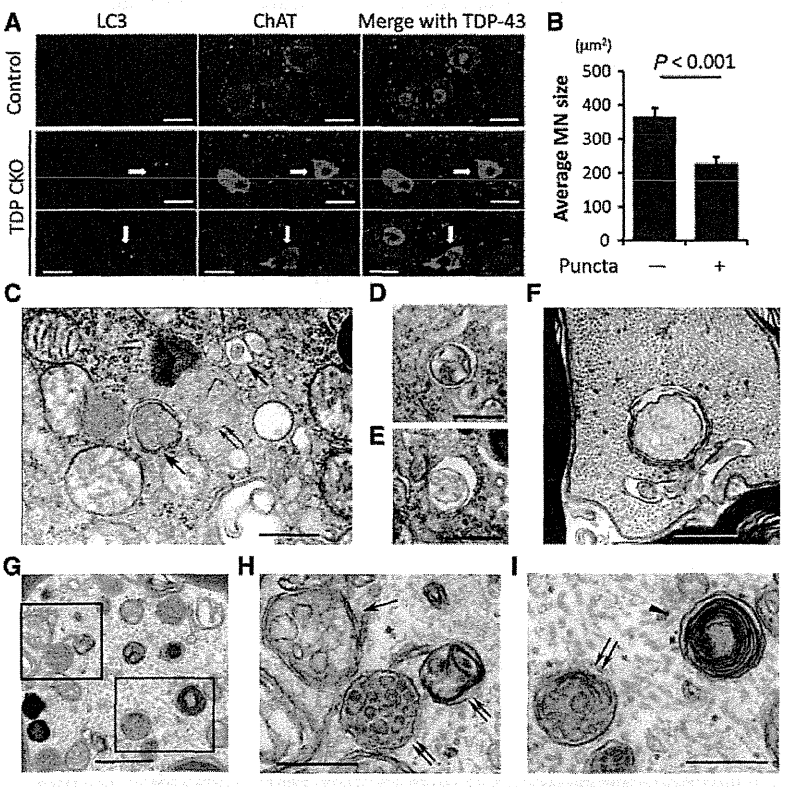

Figure 6 Formation of autophagosomes in motor neurons of TDP CKO mice. (**A**) Immunofluorescent analysis (LC3, green; ChAT, red; TDP-43, blue) revealed LC3-positive cytoplasmic puncta in TDP-43-lacking motor neurons of 100-week-old TDP CKO mice. (**B**) The average size of TDP-43 lacking motor neurons (MN) with ($n = 25$) and without ($n = 48$) LC3-positive puncta. Error bars indicate SEM. (**C–I**) Ultrastructural analysis of 100-week-old TDP CKO mice. Autophagosomes (arrows) and an autolysosome (double arrows) (**C**), autolysosomes surrounded by a single membrane containing mitochondria (**D**) and autophagosomes containing ribosome-like structures (**E**) were observed in the cell bodies of the motor neurons. An autophagic structure in the proximal motor axon (**F**). Accumulation of organelles containing mitochondria, autophagosomes (arrows), autolysosomes (double arrows), and autophagic structure with a multi-lamelleted structure (arrowhead) in the sciatic nerve (**G**) and its enlarged images (**D**, **E**, **H** and **I**). Scale bars: **A** = 20 μm; **C** and **G** = 1 μm; **F**, **H** and **I** = 500 nm.

(Fischer *et al.*, 2004). The increase of small myelinated fibres accompanied by the decrease of large myelinated fibres in the ventral root of 100-week-old TDP CKO mice corresponds to the morphological change in the cell body of the motor neurons, and similar observations were also reported in the patients and mouse models of ALS (Bradley *et al.*, 1983; Zhang *et al.*, 1997). TDP CKO mice also exhibited several features that are shared with patients with sporadic ALS: the involvement in the cranial motor nuclei such as the hypoglossal nucleus, preserved morphology in the extraocular motor neurons, accumulations of phosphorylated neurofilament in motor neurons and astrogliosis in the spinal ventral horn. Dysphagia due to the involvement of the hypoglossal nucleus might enhance the weight loss in aged TDP CKO mice through decreased oral intake. In ALS, extraocular motor neurons are resistant to degeneration compared with other somatomotor neurons, and differences in calcium buffering capacities have been proposed as a possible reason for this selective vulnerability (Alexianu *et al.*, 1994; Reiner *et al.*, 1995; Laslo *et al.*, 2000). Because RNA-seq analysis demonstrates that depletion of TDP-43 affects the calcium signalling pathway in mouse striatum (Polymenidou *et al.*, 2011), it is possible that dysregulation of calcium buffering underlies the pathogenesis of TDP CKO mice.

Our immunofluorescent analysis also demonstrated LC3-positive cytoplasmic puncta in TDP-43-depleted motor neurons, and the presence of these puncta was associated with shrinkage of motor neurons. This finding was confirmed by electron microscopy that revealed the presence of autolysosomes and autophagosomes in the motor neuronal cell bodies and axons of TDP CKO mice, suggesting that TDP-43 depletion resulted in dysregulation of the autophagic pathway. In addition, the accumulation of autophagic structures in the sciatic nerve and the disruption of retrograde labelling in TDP-43-lacking motor neurons suggest that the disruption of retrograde axonal transport may underlie the motor neuronal dysfunction in TDP CKO mice. Although the disruption of constitutive autophagy is shown to instigate the degeneration of certain types of neurons (Komatsu *et al.*, 2006), the causative role of the autophagic dysregulation in the pathogenesis of motor neuron diseases remains controversial. A recent work

demonstrates that motor neuron-specific knockout of the proteasome subunit Rpt3, but not autophagy mediator Atg7, leads to motor neuron degeneration in mice (Tashiro *et al.*, 2012), suggesting that the disruption of autophagic pathway in motor neurons may not be the primary cause of the neurodegeneration. However, accumulation of autophagosomes and autolysosomes was observed in the motor neurons of mice with mutant SOD1 (Li *et al.*, 2008; Tian *et al.*, 2011) and patients with sporadic ALS (Nakano *et al.*, 1993; Sasaki, 2011). In addition, mice carrying mutations of dynein or dynactin exhibit motor dysfunction with accumulation of autophagosomes in the motor neurons (Ravikumar *et al.*, 2005; Laird *et al.*, 2008). These lines of evidence may suggest a possible link between the increased autophagosomes and the process of motor neuron degeneration (Pasquali *et al.*, 2009; Chen *et al.*, 2012), although it remains unclear whether the accumulation of autophagosomes in neurodegenerative diseases results from activation of autophagy, disruption of retrograde transport or decreased lysosome fusion (Shintani and Klionsky, 2004; Baehrecke, 2005; Perlson *et al.*, 2010). Further investigation with regard to the linkage among loss of TDP-43, retrograde axonal transport and dysregulation of autophagy might contribute to our understanding the pathogenesis of ALS.

In conclusion, TDP CKO mice exhibited age-dependent motor impairment and morphological alterations in the motor neuron system that recapitulate several features of sporadic ALS neuropathology, including the accumulation of autophagosomes. These findings suggest that TDP-43 plays an essential role in the long-term maintenance of motor neurons, and that loss of TDP-43 function contributes to the pathogenesis of ALS.

Funding

This work was supported by a Centre of Excellence (COE) grant, a Grant in Aid for Scientific Research on Innovated Areas 'Foundation of Synapse and Neurocircuit Pathology', and Grants in-Aid from Ministry of Education, Culture, Sports, Science, and Technology (MEXT) of Japan; grants from the Ministry of Health, Labour and Welfare of Japan; and Core Research for Evolutional Science and Technology (CREST) of the Japan Science and Technology Agency (JST); Strategic Research Program for Brain Sciences of the MEXT of Japan.

Supplementary material

Supplementary material is available at *Brain* online.

References

Alexianu ME, Ho BK, Mohamed AH, La Bella V, Smith RG, Appel SH. The role of calcium-binding proteins in selective motoneuron vulnerability in amyotrophic lateral sclerosis. Ann Neurol 1994; 36: 846–58.

Arai T, Hasegawa M, Akiyama H, Ikeda K, Nonaka T, Mori H, et al. TDP-43 is a component of ubiquitin-positive tau-negative inclusions in frontotemporal lobar degeneration and amyotrophic lateral sclerosis. Biochem Biophys Res Commun 2006; 351: 602–11.

Arber S, Han B, Mendelsohn M, Smith M, Jessell TM, Sockanathan S. Requirement for the homeobox gene Hb9 in the consolidation of motor neuron identity. Neuron 1999; 23: 659–74.

Ayala YM, Misteli T, Baralle FE. TDP-43 regulates retinoblastoma protein phosphorylation through the repression of cyclin-dependent kinase 6 expression. Proc Natl Acad Sci USA 2008; 105: 3785–9.

Ayala YM, Pantano S, D'Ambrogio A, Buratti E, Brindisi A, Marchetti C, et al. Human, *Drosophila*, and *C.elegans* TDP43: nucleic acid binding properties and splicing regulatory function. J Mol Biol 2005; 348: 575–88.

Baehrecke EH. Autophagy: dual roles in life and death? Nat Rev Mol Cell Biol 2005; 6: 505–10.

Bradley WG, Good P, Rasool CG, Adelman LS. Morphometric and biochemical studies of peripheral nerves in amyotrophic lateral sclerosis. Ann Neurol 1983; 14: 267–77.

Buratti E, Brindisi A, Giombi M, Tisminetzky S, Ayala YM, Baralle FE. TDP-43 binds heterogeneous nuclear ribonucleoprotein A/B through its C-terminal tail: an important region for the inhibition of cystic fibrosis transmembrane conductance regulator exon 9 splicing. J Biol Chem 2005; 280: 37572–84.

Buratti E, De Conti L, Stuani C, Romano M, Baralle M, Baralle F. Nuclear factor TDP-43 can affect selected microRNA levels. FEBS J 2010; 277: 2268–81.

Chen S, Zhang X, Song L, Le W. Autophagy dysregulation in amyotrophic lateral sclerosis. Brain Pathol 2012; 22: 110–6.

Chiang PM, Ling J, Jeong YH, Price DL, Aja SM, Wong PC. Deletion of TDP-43 down-regulates Tbc1d1, a gene linked to obesity, and alters body fat metabolism. Proc Natl Acad Sci USA 2010; 107: 16320–4.

Feiguin F, Godena VK, Romano G, D'Ambrogio A, Klima R, Baralle FE. Depletion of TDP-43 affects *Drosophila* motoneurons terminal synapsis and locomotive behavior. FEBS Lett 2009; 583: 1586–92.

Fischer LR, Culver DG, Tennant P, Davis AA, Wang M, Castellano-Sanchez A, et al. Amyotrophic lateral sclerosis is a distal axonopathy: evidence in mice and man. Exp Neurol 2004; 185: 232–40.

Gitcho MA, Baloh RH, Chakraverty S, Mayo K, Norton JB, Levitch D, et al. TDP-43 A315T mutation in familial motor neuron disease. Ann Neurol 2008; 63: 535–8.

Igaz LM, Kwong LK, Lee EB, Chen-Plotkin A, Swanson E, Unger T, et al. Dysregulation of the ALS-associated gene TDP-43 leads to neuronal death and degeneration in mice. J Clin Invest 2011; 121: 726–38.

Iguchi Y, Katsuno M, Niwa J, Yamada S, Sone J, Waza M, et al. TDP-43 depletion induces neuronal cell damage through dysregulation of Rho family GTPases. J Biol Chem 2009; 284: 22059–66.

Kabashi E, Lin L, Tradewell ML, Dion PA, Bercier V, Bourgouin P, et al. Gain and loss of function of ALS-related mutations of TARDBP (TDP-43) cause motor deficits *in vivo*. Hum Mol Genet 2011; 19: 671–83.

Kabashi E, Valdmanis PN, Dion P, Spiegelman D, McConkey BJ, Vande Velde C, et al. TARDBP mutations in individuals with sporadic and familial amyotrophic lateral sclerosis. Nat Genet 2008; 40: 572–4.

Katsuno M, Adachi H, Kume A, Li M, Nakagomi Y, Niwa H, et al. Testosterone reduction prevents phenotypic expression in a transgenic mouse model of spinal and bulbar muscular atrophy. Neuron 2002; 35: 843–54.

Katsuno M, Adachi H, Minamiyama M, Waza M, Tokui K, Banno H, et al. Reversible disruption of dynactin 1-mediated retrograde axonal transport in polyglutamine-induced motor neuron degeneration. J Neurosci 2006; 26: 12106–17.

Komatsu M, Waguri S, Chiba T, Murata S, Iwata J, Tanida I, et al. Loss of autophagy in the central nervous system causes neurodegeneration in mice. Nature 2006; 441: 880–4.

Kraemer BC, Schuck T, Wheeler JM, Robinson LC, Trojanowski JQ, Lee VM, et al. Loss of murine TDP-43 disrupts motor function and plays an essential role in embryogenesis. Acta Neuropathol 2010; 119: 409–19.

Laird FM, Farah MH, Ackerley S, Hoke A, Maragakis N, Rothstein JD, et al. Motor neuron disease occurring in a mutant dynactin mouse

model is characterized by defects in vesicular trafficking. J Neurosci 2008; 28: 1997–2005.
Laslo P, Lipski J, Nicholson LF, Miles GB, Funk GD. Calcium binding proteins in motoneurons at low and high risk for degeneration in ALS. Neuroreport 2000; 11: 3305–8.
Lee EB, Lee VM, Trojanowski JQ. Gains or losses: molecular mechanisms of TDP43-mediated neurodegeneration. Nat Rev Neurosci 2011; 13: 38–50.
Li L, Zhang X, Le W. Altered macroautophagy in the spinal cord of SOD1 mutant mice. Autophagy 2008; 4: 290–3.
Misawa H, Nakata K, Toda K, Matsuura J, Oda Y, Inoue H, et al. VAChT-Cre. Fast and VAChT-Cre.Slow: postnatal expression of Cre recombinase in somatomotor neurons with different onset. Genesis 2003; 37: 44–50.
Nakano I, Shibata T, Uesaka Y. On the possibility of autolysosomal processing of skein-like inclusions. Electron microscopic observation in a case of amyotrophic lateral sclerosis. J Neurol Sci 1993; 120: 54–9.
Neumann M, Sampathu DM, Kwong LK, Truax AC, Micsenyi MC, Chou TT, et al. Ubiquitinated TDP-43 in frontotemporal lobar degeneration and amyotrophic lateral sclerosis. Science 2006; 314: 130–3.
Pasquali L, Longone P, Isidoro C, Ruggieri S, Paparelli A, Fornai F. Autophagy, lithium, and amyotrophic lateral sclerosis. Muscle Nerve 2009; 40: 173–94.
Perlson E, Maday S, Fu MM, Moughamian AJ, Holzbaur EL. Retrograde axonal transport: pathways to cell death? Trends Neurosci 2010; 33: 335–44.
Polymenidou M, Lagier-Tourenne C, Hutt KR, Huelga SC, Moran J, Liang TY, et al. Long pre-mRNA depletion and RNA missplicing contribute to neuronal vulnerability from loss of TDP-43. Nat Neurosci 2011; 14: 459–68.
Ravikumar B, Acevedo-Arozena A, Imarisio S, Berger Z, Vacher C, O'Kane CJ, et al. Dynein mutations impair autophagic clearance of aggregate-prone proteins. Nat Genet 2005; 37: 771–6.
Reiner A, Medina L, Figueredo-Cardenas G, Anfinson S. Brainstem motoneuron pools that are selectively resistant in amyotrophic lateral sclerosis are preferentially enriched in parvalbumin: evidence from monkey brainstem for a calcium-mediated mechanism in sporadic ALS. Exp Neurol 1995; 131: 239–50.
Sasaki S. Autophagy in spinal cord motor neurons in sporadic amyotrophic lateral sclerosis. J Neuropathol Exp Neurol 2011; 70: 349–59.
Sephton CF, Cenik C, Kucukural A, Dammer EB, Cenik B, Han Y, et al. Identification of neuronal RNA targets of TDP-43-containing ribonucleoprotein complexes. J Biol Chem 2011; 286: 1204–15.
Sephton CF, Good SK, Atkin S, Dewey CM, Mayer P III, Herz J, et al. TDP-43 is a developmentally regulated protein essential for early embryonic development. J Biol Chem 2010; 285: 6826–34.
Shan X, Chiang PM, Price DL, Wong PC. Altered distributions of Gemini of coiled bodies and mitochondria in motor neurons of TDP-43 transgenic mice. Proc Natl Acad Sci USA 2010; 107: 16325–30.
Shintani T, Klionsky DJ. Autophagy in health and disease: a double-edged sword. Science 2004; 306: 990–5.
Sreedharan J, Blair IP, Tripathi VB, Hu X, Vance C, Rogelj B, et al. TDP-43 mutations in familial and sporadic amyotrophic lateral sclerosis. Science 2008; 319: 1668–72.
Stallings NR, Puttaparthi K, Luther CM, Burns DK, Elliott JL. Progressive motor weakness in transgenic mice expressing human TDP-43. Neurobiol Dis 2010; 40: 404–14.
Strong MJ, Volkening K, Hammond R, Yang W, Strong W, Leystra-Lantz C, et al. TDP43 is a human low molecular weight neurofilament (hNFL) mRNA-binding protein. Mol Cell Neurosci 2007; 35: 320–7.
Swarup V, Phaneuf D, Bareil C, Robertson J, Rouleau GA, Kriz J, et al. Pathological hallmarks of amyotrophic lateral sclerosis/frontotemporal lobar degeneration in transgenic mice produced with TDP-43 genomic fragments. Brain 2011; 134: 2610–26.
Tashiro Y, Urushitani M, Inoue H, Koike M, Uchiyama Y, Komatsu M, et al. Motor neuron-specific disruption of proteasomes, but not autophagy, replicates amyotrophic lateral sclerosis. J Biol Chem 2012; 287: 42984–94.
Tian F, Morimoto N, Liu W, Ohta Y, Deguchi K, Miyazaki K, et al. *In vivo* optical imaging of motor neuron autophagy in a mouse model of amyotrophic lateral sclerosis. Autophagy 2011; 7: 985–92.
Tollervey JR, Curk T, Rogelj B, Briese M, Cereda M, Kayikci M, et al. Characterizing the RNA targets and position-dependent splicing regulation by TDP-43. Nat Neurosci 2011; 14: 452–8.
Tsai KJ, Yang CH, Fang YH, Cho KH, Chien WL, Wang WT, et al. Elevated expression of TDP-43 in the forebrain of mice is sufficient to cause neurological and pathological phenotypes mimicking FTLD-U. J Exp Med 2010; 207: 1661–73.
Uchida A, Sasaguri H, Kimura N, Tajiri M, Ohkubo T, Ono F, et al. Non-human primate model of amyotrophic lateral sclerosis with cytoplasmic mislocalization of TDP-43. Brain 2012; 135: 833–46.
Wang HY, Wang IF, Bose J, Shen CK. Structural diversity and functional implications of the eukaryotic TDP gene family. Genomics 2004; 83: 130–9.
Wegorzewska I, Bell S, Cairns NJ, Miller TM, Baloh RH. TDP-43 mutant transgenic mice develop features of ALS and frontotemporal lobar degeneration. Proc Natl Acad Sci USA 2009; 106: 18809–14.
Wils H, Kleinberger G, Janssens J, Pereson S, Joris G, Cuijt I, et al. TDP-43 transgenic mice develop spastic paralysis and neuronal inclusions characteristic of ALS and frontotemporal lobar degeneration. Proc Natl Acad Sci USA 2010; 107: 3858–63.
Wu LS, Cheng WC, Hou SC, Yan YT, Jiang ST, Shen CK. TDP-43, a neuro-pathosignature factor, is essential for early mouse embryogenesis. Genesis 2010; 48: 56–62.
Wu LS, Cheng WC, Shen CK. Targeted Depletion of TDP-43 Expression in the spinal cord motor neurons leads to the development of Amyotrophic Lateral Sclerosis (ALS)-like phenotypes in mice. J Biol Chem 2012; 287: 27335–44.
Xu YF, Gendron TF, Zhang YJ, Lin WL, D'Alton S, Sheng H, et al. Wild-type human TDP-43 expression causes TDP-43 phosphorylation, mitochondrial aggregation, motor deficits, and early mortality in transgenic mice. J Neurosci 2010; 30: 10851–9.
Yokoseki A, Shiga A, Tan CF, Tagawa A, Kaneko H, Koyama A, et al. TDP-43 mutation in familial amyotrophic lateral sclerosis. Ann Neurol 2008; 63: 538–42.
Zhang B, Tu P, Abtahian F, Trojanowski JQ, Lee VM. Neurofilaments and orthograde transport are reduced in ventral root axons of transgenic mice that express human SOD1 with a G93A mutation. J Cell Biol 1997; 139: 1307–15.
Zhou H, Huang C, Chen H, Wang D, Landel CP, Xia PY, et al. Transgenic rat model of neurodegeneration caused by mutation in the TDP gene. PLoS Genet 2010; 6: e1000887.

nature medicine

Naratriptan mitigates CGRP1-associated motor neuron degeneration caused by an expanded polyglutamine repeat tract

Makoto Minamiyama[1,3], Masahisa Katsuno[1,3], Hiroaki Adachi[1], Hideki Doi[1], Naohide Kondo[1], Madoka Iida[1], Shinsuke Ishigaki[1], Yusuke Fujioka[1], Shinjiro Matsumoto[1], Yu Miyazaki[1], Fumiaki Tanaka[1], Hiroki Kurihara[2] & Gen Sobue[1]

Spinal and bulbar muscular atrophy (SBMA) is a motor neuron disease caused by the expansion of the CAG triplet repeat within the androgen receptor (*AR*) gene. Here, we demonstrated that pathogenic AR upregulates the gene encoding calcitonin gene-related peptide α (CGRP1). In neuronal cells, overexpression of CGRP1 induced cellular damage via the activation of the c-Jun N-terminal kinase (JNK) pathway, whereas pharmacological suppression of CGRP1 or JNK attenuated the neurotoxic effects of pathogenic AR. The depletion of CGRP1 inactivated JNK and suppressed neurodegeneration in a mouse model of SBMA. Naratriptan, a serotonin 1B/1D (5-hydroxytryptamine 1B/1D, or 5-HT1B/1D) receptor agonist, decreased CGRP1 expression via the induction of dual-specificity protein phosphatase 1 (DUSP1), attenuated JNK activity and mitigated pathogenic AR-mediated neuronal damage in cellular and mouse SBMA models. These observations suggest that pharmacological activation of the 5-HT1B/1D receptor may be used therapeutically to treat SBMA and other polyglutamine-related neurodegenerative diseases.

The expansion of a genomic trinucleotide CAG repeat causes hereditary neurodegenerative disorders such as Huntington's disease, SBMA, dentatorubral-pallidoluysian atrophy and six forms of spinocerebellar ataxia[1,2]. SBMA, or Kennedy's disease, is a late-onset motor neuron disease characterized by progressive weakness and atrophy of bulbar, facial and limb muscles, which is attributable to the degeneration of lower motor neurons in the spinal cord and brainstem[3,4]. This disease is caused by an abnormal expansion of CAG repeats encoding the amino acid glutamine within the gene encoding AR, and it exclusively affects males carrying this type of mutation[5,6]. The pathogenic AR protein accumulates in the nucleus of motor neurons and causes several molecular changes, including transcriptional dysregulation, axonal transport defects, mitochondrial dysfunction and disruption of the transforming growth factor-β signaling pathway[7–17].

Dysregulation of the transcriptional machinery associated with histone hypoacetylation has been reported in cellular and animal models of polyglutamine diseases[18,19]. In addition to downregulation of genes that are necessary for the maintenance of normal cellular function, upregulation of certain molecules has also been observed in affected tissues in polyglutamine diseases[20,21]. These alterations of the normal gene expression profile seem to mediate polyglutamine toxicity in neuronal and non-neuronal cells and are partially reversed by histone acetylation[14,22,23]. However, it is unknown which genes are dysregulated and directly contribute to neurodegeneration.

Here, we performed a microarray analysis of the spinal cord of a mouse model of SBMA to identify the changes in gene expression that play a crucial part in polyglutamine-mediated neurodegeneration. We also examined whether genetic and pharmacological modulation of the expression of the identified genes could mitigate the histopathological and symptomatic effects of motor neuron degeneration.

RESULTS

Calcitonin gene–related peptide is upregulated in SBMA

To identify the gene expression changes that are specific to SBMA, we prepared total mRNA samples from the spinal cords of transgenic mice carrying a full-length human AR with 97 CAGs (AR-97Q), transgenic mice bearing a wild-type allele of AR with 24 CAGs (AR-24Q) and the wild-type littermates of the AR-97Q mice. Using microarray analysis, we identified genes with significantly altered expression among the three types of mice ($P < 0.005$). The expression of 124 genes were increased (>150%) or decreased (<67%) in male AR-97Q mice compared with their AR-24Q counterparts at the before-onset stage (7–9 weeks old). The expression of 12 of the 124 genes also showed a considerable difference between the AR-97Q and wild-type littermates but not between the AR-24Q and wild-type littermates (**Fig. 1a** and **Supplementary Table 1**). Among these candidates, we focused on the gene encoding calcitonin gene-related peptide 1 (Cgrp1) for the following reasons: (i) this gene, *Calca*, was

[1]Department of Neurology, Nagoya University Graduate School of Medicine, Nagoya, Japan. [2]Department of Physiological Chemistry and Metabolism, Graduate School of Medicine, University of Tokyo, Tokyo, Japan. [3]These authors contributed equally to this work. Correspondence should be addressed to M.K. (ka2no@med.nagoya-u.ac.jp) or G.S. (sobueg@med.nagoya-u.ac.jp).

Received 28 December 2011; accepted 13 August 2012; published online 30 September 2012; doi:10.1038/nm.2932

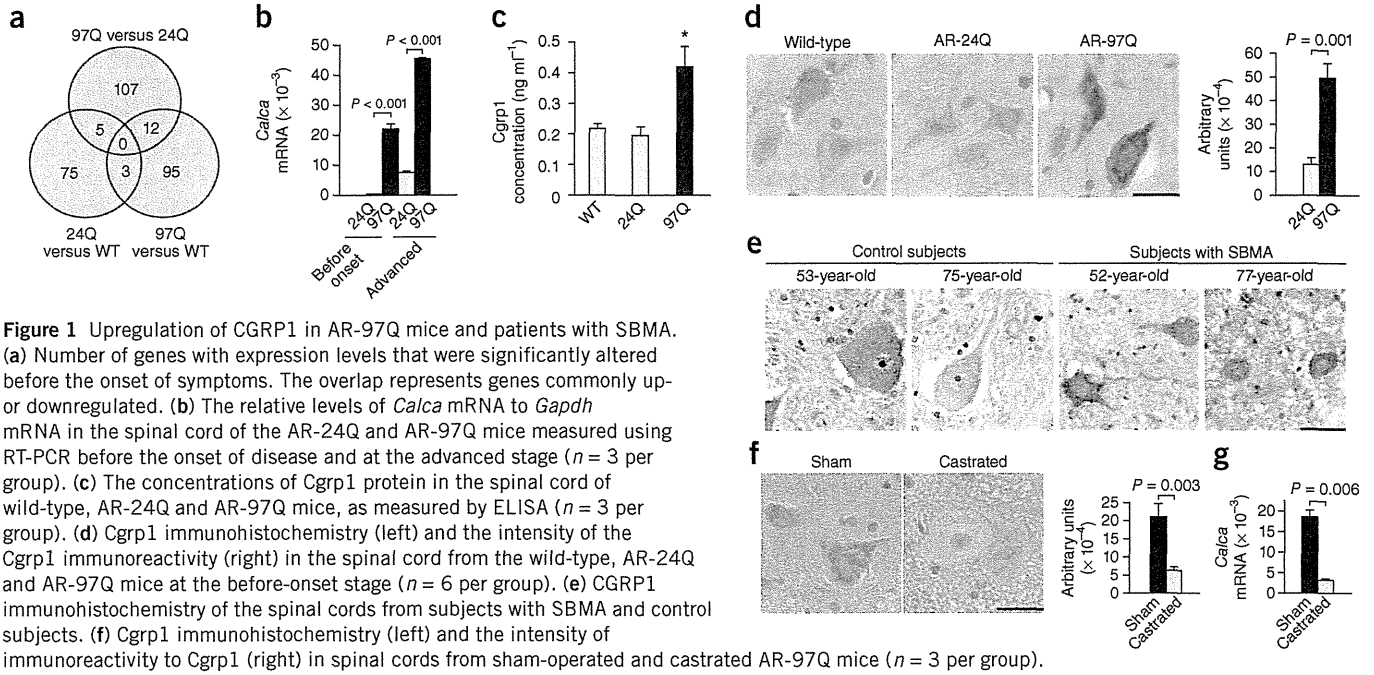

Figure 1 Upregulation of CGRP1 in AR-97Q mice and patients with SBMA. (**a**) Number of genes with expression levels that were significantly altered before the onset of symptoms. The overlap represents genes commonly up- or downregulated. (**b**) The relative levels of *Calca* mRNA to *Gapdh* mRNA in the spinal cord of the AR-24Q and AR-97Q mice measured using RT-PCR before the onset of disease and at the advanced stage ($n = 3$ per group). (**c**) The concentrations of Cgrp1 protein in the spinal cord of wild-type, AR-24Q and AR-97Q mice, as measured by ELISA ($n = 3$ per group). (**d**) Cgrp1 immunohistochemistry (left) and the intensity of the Cgrp1 immunoreactivity (right) in the spinal cord from the wild-type, AR-24Q and AR-97Q mice at the before-onset stage ($n = 6$ per group). (**e**) CGRP1 immunohistochemistry of the spinal cords from subjects with SBMA and control subjects. (**f**) Cgrp1 immunohistochemistry (left) and the intensity of immunoreactivity to Cgrp1 (right) in spinal cords from sham-operated and castrated AR-97Q mice ($n = 3$ per group). (**g**) The levels of *Calca* mRNA in spinal cords of sham-operated and castrated AR-97Q mice at the advanced stage ($n = 3$ per group). The scale bars indicate 20 μm (**d**,**e**) or 50 μm (**f**). The error bars indicate the s.e.m. $^*P < 0.05$ by analysis of variance (ANOVA) and Dunnett's test (**c**).

significantly upregulated in the AR-97Q mice compared with the other types of mice; (ii) the expression of this gene showed a further increase at the advanced stage (13–15 weeks old) (**Supplementary Table 1**); and (iii) this gene is expressed chiefly in lower motor neurons and dorsal root ganglion sensory neurons, not in glial or vascular endothelial cells[24]. We confirmed the results of the microarray using RT-PCR, which also showed strain- and stage-dependent upregulation of *Calca* mRNA (**Fig. 1b**).

The concentration of Cgrp1 in spinal cord tissue measured by ELISA was significantly higher in AR-97Q mice compared with AR-24Q or wild-type counterparts (**Fig. 1c**). Immunohistochemistry with Cgrp1-specific antibodies showed that Cgrp1 immunoreactivity

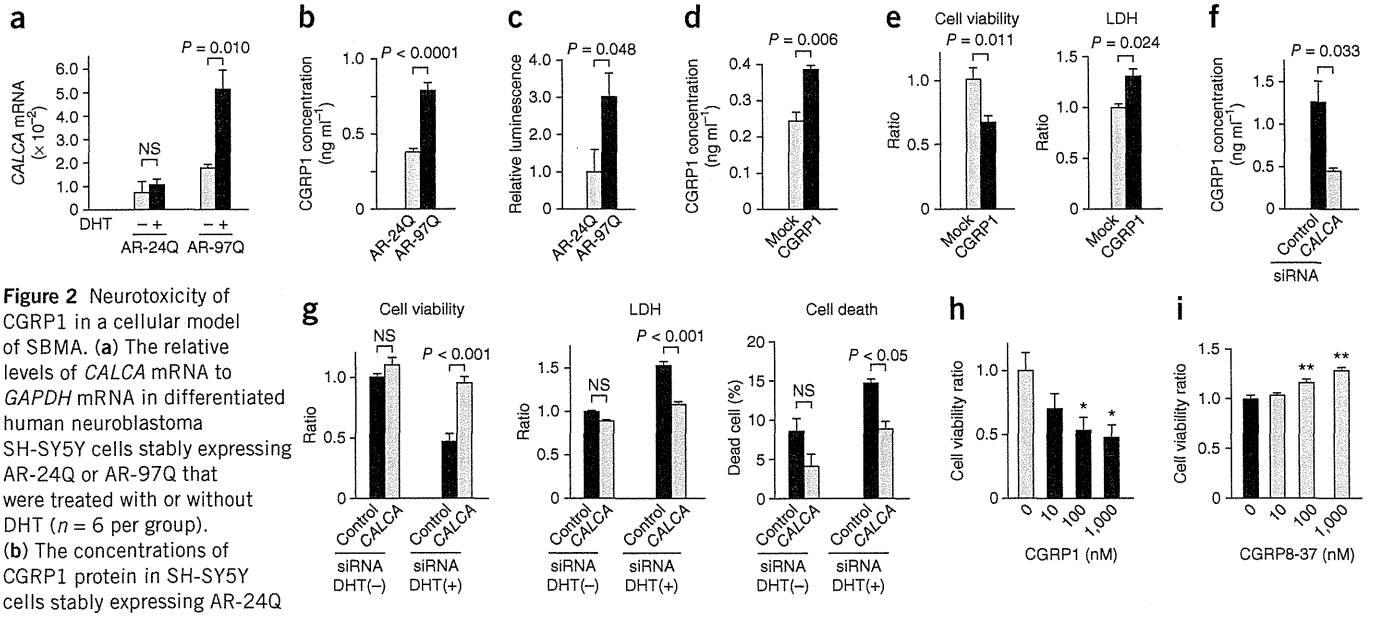

Figure 2 Neurotoxicity of CGRP1 in a cellular model of SBMA. (**a**) The relative levels of *CALCA* mRNA to *GAPDH* mRNA in differentiated human neuroblastoma SH-SY5Y cells stably expressing AR-24Q or AR-97Q that were treated with or without DHT ($n = 6$ per group). (**b**) The concentrations of CGRP1 protein in SH-SY5Y cells stably expressing AR-24Q or AR-97Q. (**c**) Luciferase activity transcriptionally regulated by the *CALCA* promoter in SH-SY5Y cells stably expressing AR-24Q or AR-97Q ($n = 6$ per group). (**d**) The concentrations of CGRP1 protein in SH-SY5Y cells transfected with a mock or CGRP1 vector ($n = 3$). (**e**) The viability as measured by cell viability WST-1 assay (left) and LDH release (right) of SH-SY5Y cells transfected with mock or CGRP1 vector ($n = 6$ per group). (**f**) The levels of CGRP1 protein in SH-SY5Y cells stably expressing AR-97Q transfected with control or *CALCA* siRNA ($n = 3$ per group). (**g**) The viability, LDH release and cell death (measured by Trypan blue dye exclusion) of SH-SY5Y cells stably expressing AR-97Q that were transfected with control or *CALCA* siRNA and treated with or without DHT ($n = 6$ per group). (**h**) The viability of SH-SY5Y cells treated with or without synthetic CGRP1 ($n = 6$ per group). (**i**) The viability of SH-SY5Y cells stably expressing AR-97Q treated with or without CGRP8-37, a CGRP1 receptor antagonist ($n = 6$ per group). $^*P < 0.05$ and $^{**}P < 0.01$ by ANOVA with Dunnett's test (**h**,**i**). The error bars indicate the s.e.m. NS, not significant.

in the spinal motor neurons was significantly stronger in the AR-97Q mice at both the before-onset and advanced stages (**Fig. 1d** and **Supplementary Fig. 1a,b**). Although we also detected Cgrp1 in the spinal dorsal horn, the expression of Cgrp1 was not different among the AR-97Q, AR-24Q and wild-type mice (data not shown). Cgrp1 is also expressed in other regions of the central nervous system, although the expression levels in these tissues are much lower than in the spinal cord (**Supplementary Fig. 2a**). Besides the spinal motor neurons, hypoglossal motor neurons and cerebellar granular cells also had high expression of Cgrp1, which accumulated in the cytoplasm of neurons with nuclear accumulation of the pathogenic AR (**Supplementary Fig. 2b,c**). Moreover, immunohistochemical analysis of autopsied human specimens showed higher expression of CGRP1 in the spinal motor neurons of subjects with SBMA compared to controls (**Fig. 1e** and **Supplementary Fig. 3a,b**). Because surgical or pharmacological suppression of testosterone release ameliorates the symptomatic and neuropathological changes in male AR-97Q mice[11,25], we examined the effects of the male sex hormone on the expression of CGRP1 in the mice. Surgical castration significantly decreased the immunoreactivity of Cgrp1 in the male AR-97Q mice (**Fig. 1f**), which is consistent with prior reports demonstrating the expression of CGRP1 is negatively regulated by testosterone[26]. The mRNA levels of *Calca* also decreased as a result of the castration (**Fig. 1g**).

CGRP1 mediates polyglutamine-dependent cytotoxicity

We further investigated the role of CGRP1 in polyglutamine-mediated neurotoxicity in differentiated human neuroblastoma SH-SY5Y cells stably expressing human AR containing 24 or 97 glutamines (AR-24Q and AR-97Q). In this cellular model, polyglutamine-expanded AR induced neurotoxicity and cell death in a testosterone-dependent manner (**Supplementary Fig. 4a–f**). In agreement with the data from the mouse model, cells expressing AR-97Q that were treated with dihydrotestosterone (DHT) had higher levels of *CALCA* mRNA than those bearing AR-24Q (**Fig. 2a**). SH-SY5Y cells expressing the pathogenic AR had higher protein amounts of CGRP1 and luciferase activity under control of the *CALCA* promoter (**Fig. 2b,c**).

We next investigated the relationship between expression of CGRP1 and viability of neuronal cells. Transient overexpression of CGRP1 in SH-SY5Y cells reduced viability and increased cellular damage as measured by the lactate dehydrogenase (LDH) assay (**Fig. 2d,e**). In contrast, siRNA-mediated knockdown of *CALCA* expression diminished the damage and death of cells stably expressing AR-97Q that were treated with DHT (**Fig. 2f,g**). CGRP1 is secreted from neurons, binds its receptors on the cell surface and functions as an autocrine and paracrine factor[27]. We thus examined the effect of CGRP1 on cellular viability via stimulation of its receptor. Administration of synthetic CGRP1 peptides dose-dependently decreased the viability of SH-SY5Y cells (**Fig. 2h**). In contrast, treatment with CGRP8-37, which is an antagonist of the CGRP receptor, attenuated the cytotoxicity caused by the pathogenic AR (**Fig. 2i**).

To confirm the result obtained in SH-SY5Y cell line, we examined the levels of Cgrp1 in mouse primary motor neurons infected with lentiviral vectors containing an N-terminal fragment of human AR with 24 or 97 glutamines (AR-24Q and AR-97Q)[17]. The pathogenic AR formed aggregates (**Supplementary Fig. 5a**) and increased the

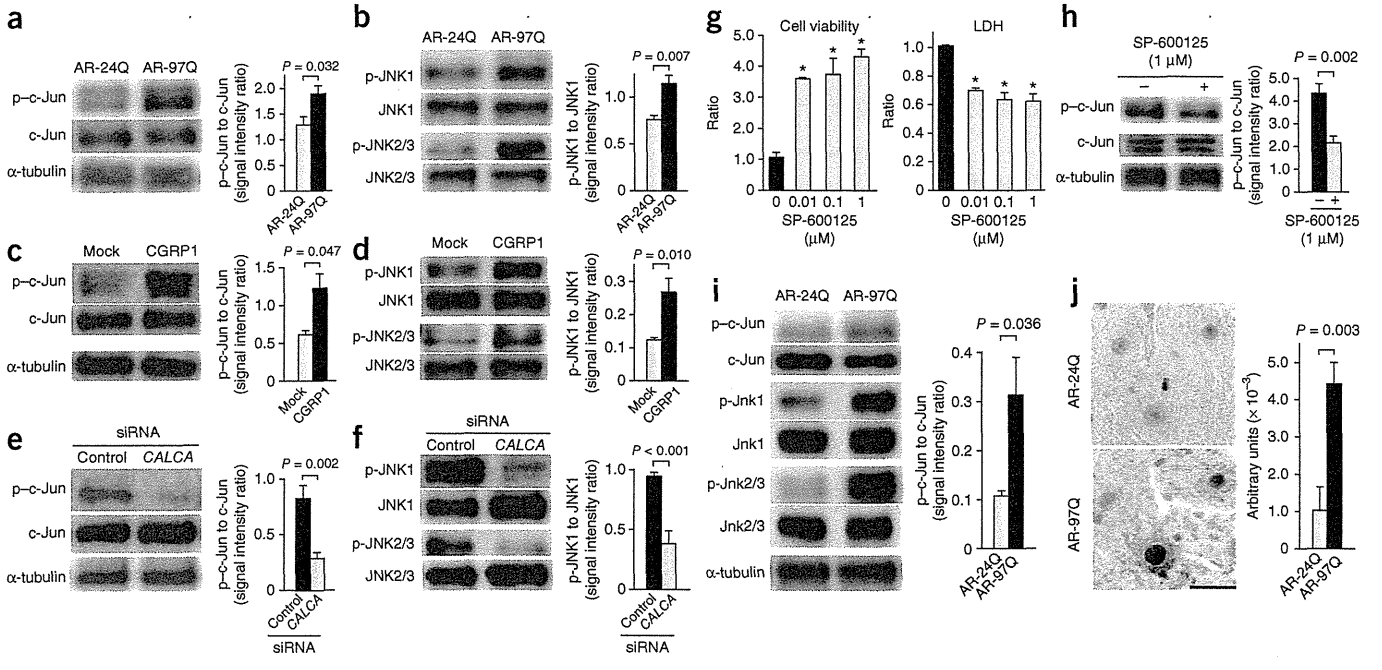

Figure 3 CGRP1 induces neuronal cell damage via activation of the JNK pathway. (**a,b**) Immunoblots for c-Jun (**a**) and JNK (**b**) and the relative intensities of immunoreactive bands from SH-SY5Y cells stably expressing AR-24Q and AR-97Q ($n = 6$ per group). (**c,d**) Immunoblots for c-Jun (**c**) and JNK (**d**) and the relative intensities of immunoreactive bands from SH-SY5Y cells transfected with the mock or CGRP1 vector ($n = 6$ per group). (**e,f**) Immunoblots for c-Jun (**e**) and JNK (**f**) and the relative intensities of immunoreactive bands from SH-SY5Y cells stably expressing AR-97Q transfected with control and *CALCA* siRNA ($n = 6$ per group). (**g**) The viability of (left) and LDH release from (right) SH-SY5Y cells stably expressing AR-97Q treated with a JNK inhibitor, SP-600125 ($n = 6$ per group). (**h**) Immunoblots and relative intensities of p–c-Jun immunoreactive bands from SH-SY5Y cells stably expressing AR-97Q and treated with SP-600125 ($n = 6$ per group). (**i**) Immunoblots (left) and the relative signal intensities (right) of the p–c-Jun immunoreactive bands for spinal cords from the AR-24Q and AR-97Q mice ($n = 6$ per group). (**j**) p–c-Jun immunohistochemistry (left) and the intensity of immunoreactivity to p–c-Jun (right) in spinal motor neurons of AR-24Q and AR-97Q mice ($n = 6$ per group). The scale bar indicates 20 μm. The error bars indicate the s.e.m. $^*P < 0.01$ by ANOVA with Dunnett's test (**g**).

mRNA levels of *Calca* in motor neurons (**Supplementary Fig. 5b**). Furthermore, administration of CGRP1 peptides decreased the viability of primary motor neurons (**Supplementary Fig. 5c**).

CGRP1 induces toxicity via the activation of c-Jun

CGRP1 is known to regulate various cellular signaling pathways, such as nuclear factor-κB (NF-κB) and JNK[28]. We next investigated the molecular mechanism by which CGRP1 elicited neuronal damage (**Supplementary Note** and **Supplementary Fig. 6a–c**). We found that AR-97Q increases the phosphorylation of c-Jun and JNK in neuronal cells treated with DHT (**Fig. 3a,b** and **Supplementary Figs. 7** and **8a**). We also observed activation of the JNK pathway by pathogenic AR in primary motor neurons (**Supplementary Fig. 8b**). Overexpression of CGRP1 also enhanced activation of the JNK pathway in SH-SY5Y cells (**Fig. 3c,d** and **Supplementary Fig. 7b,f**).

To determine whether pathogenic AR stimulates the JNK pathway via the upregulation of CGRP1, we knocked down expression of *CALCA* using siRNA in SH-SY5Y cells stably expressing AR-97Q that are treated with DHT. Transfection of *CALCA* siRNA suppressed activation of the JNK pathway (**Fig. 3e,f** and **Supplementary Fig. 7c,g**). Furthermore, pharmacological inhibition of JNK by SP-600125 increased cell viability and suppressed cytotoxic damage in SH-SY5Y cells stably expressing AR-97Q (**Fig. 3g,h**) and in those treated with CGRP1 peptides (**Supplementary Fig. 8c**). Immunoblot and histopathological analyses also demonstrated activation of the JNK pathway in the AR-97Q mice (**Fig. 3i,j** and **Supplementary Fig. 7d**).

Calca depletion ameliorates motor neuron degeneration

To clarify the role of CGRP1 in the pathogenic processes of SBMA, we next investigated the biological effects of depletion of *Calca* in male AR-97Q mice. Homozygous deletion of the *Calca* gene improved motor function, as assessed by the rotarod task and grip strength, increased body weight and extended the lifespan of the AR-97Q *Calca*$^{-/-}$ mice (**Fig. 4a**). We confirmed that the Cgrp1 protein was depleted in the spinal motor neurons of male AR-97Q *Calca*$^{-/-}$ mice (**Fig. 4b,c**). Histopathological analyses of the skeletal muscles showed that neurogenic amyotrophy was attenuated by depletion of *Calca* (**Fig. 4d**).

Depletion of *Calca* mitigated reactive astrogliosis in the spinal cord of AR-97Q mice, as assessed by GFAP staining at the advanced stage (**Fig. 4e**). Depletion of *Calca* also upregulated the expression of choline acetyltransferase (ChAT), a marker of motor neuronal function (**Fig. 4f,g**). We confirmed that *Calca* depletion had no detectable effects on motor function or ChAT expression in wild-type mice (**Supplementary Fig. 9a–h**). In addition, histopathological and immunoblot analyses showed that deletion of the *Calca* gene suppressed the phosphorylation of c-Jun in the spinal motor neurons of male AR-97Q mice (**Fig. 4h** and **Supplementary Fig. 9i**).

CGRP1 suppression mitigates polyglutamine toxicity

CGRP1 has been implicated in the molecular pathogenesis of migraines, and 5-HT1B/1D receptor agonists have been shown to suppress the expression and secretion of CGRP1 in neurons[29]. We thus determined whether these antimigraine drugs could alleviate polyglutamine-mediated neurotoxicity by decreasing the expression of CGRP1 in neuronal cells. The 5-HT1B/1D receptor agonists sumatriptan, naratriptan and rizatriptan reduced the cellular damage and restored the viability of SH-SY5Y cells that stably expressed AR-97Q (**Fig. 5a**). Given that naratriptan has the longest half-life among these drugs, it may be an appropriate candidate for the treatment

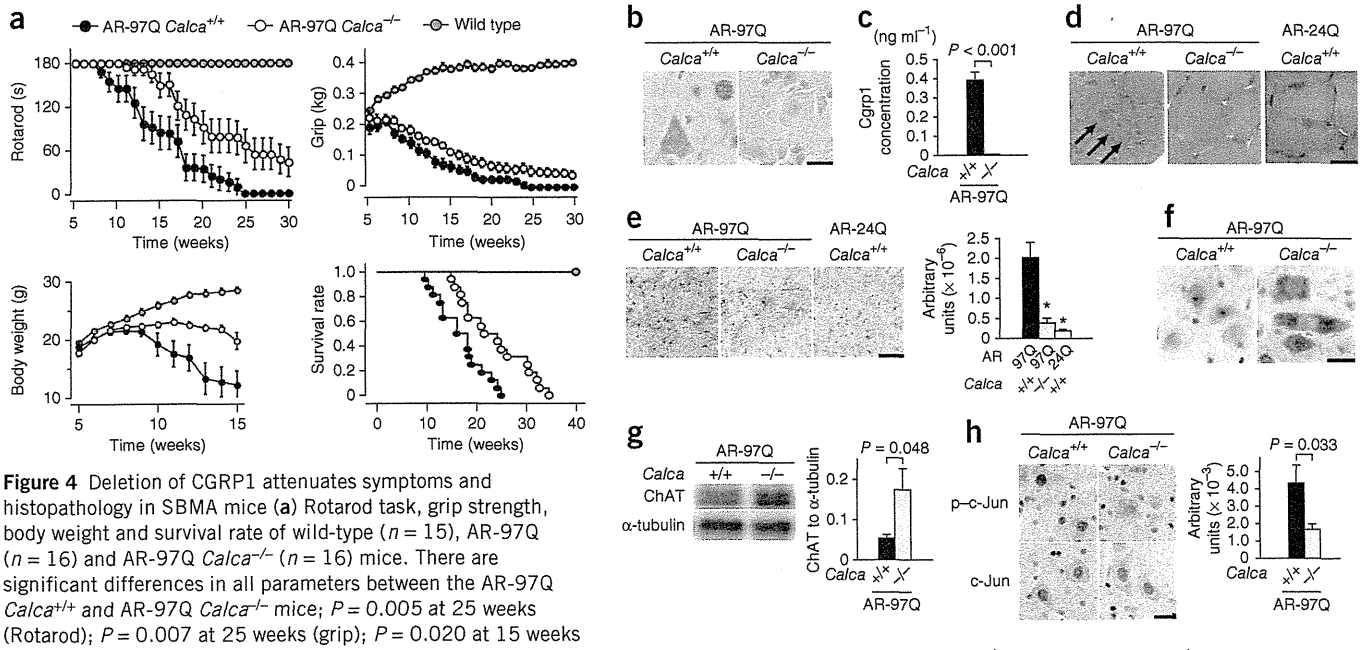

Figure 4 Deletion of CGRP1 attenuates symptoms and histopathology in SBMA mice (**a**) Rotarod task, grip strength, body weight and survival rate of wild-type ($n = 15$), AR-97Q ($n = 16$) and AR-97Q *Calca*$^{-/-}$ ($n = 16$) mice. There are significant differences in all parameters between the AR-97Q *Calca*$^{+/+}$ and AR-97Q *Calca*$^{-/-}$ mice; $P = 0.005$ at 25 weeks (Rotarod); $P = 0.007$ at 25 weeks (grip); $P = 0.020$ at 15 weeks (body weight); and $P = 0.003$ (survival). (**b**) Cgrp1 immunohistochemistry of spinal cords from AR-97Q *Calca*$^{+/+}$ and AR-97Q *Calca*$^{-/-}$ mice (15 weeks old). (**c**) The concentrations of Cgrp1 protein in the spinal cord of AR-97Q *Calca*$^{+/+}$ and AR-97Q *Calca*$^{-/-}$ mice as measured by ELISA ($n = 3$ per group). (**d**) H&E staining of skeletal muscle from AR-97Q *Calca*$^{+/+}$, AR-97Q *Calca*$^{-/-}$ and AR-24Q mice. (**e**) Gfap immunohistochemistry (left) and intensity of immunoreactivity to Gfap (right) in spinal cord sections from AR-97Q *Calca*$^{+/+}$, AR-97Q *Calca*$^{-/-}$ and AR-24Q mice ($n = 6$ per group). (**f**) ChAT immunohistochemistry in spinal cord sections from AR-97Q *Calca*$^{+/+}$ and AR-97Q *Calca*$^{-/-}$ mice. (**g**) Immunoblots (left) and relative signal intensities of ChAT-immunoreactive bands (right) of spinal cords from the AR-97Q *Calca*$^{+/+}$ and AR-97Q *Calca*$^{-/-}$ mice ($n = 6$ per group). (**h**) c-Jun immunohistochemistry (left) and intensity of immunoreactivity to p–c-Jun (right) in spinal cords from AR-97Q *Calca*$^{+/+}$ and AR-97Q *Calca*$^{-/-}$ mice ($n = 6$ per group). The scale bars indicate 20 μm (**b**,**f**,**h**) or 50 μm (**d**,**e**). The error bars indicate the s.e.m. $^*P < 0.01$ by ANOVA with Dunnett's test (**e**).

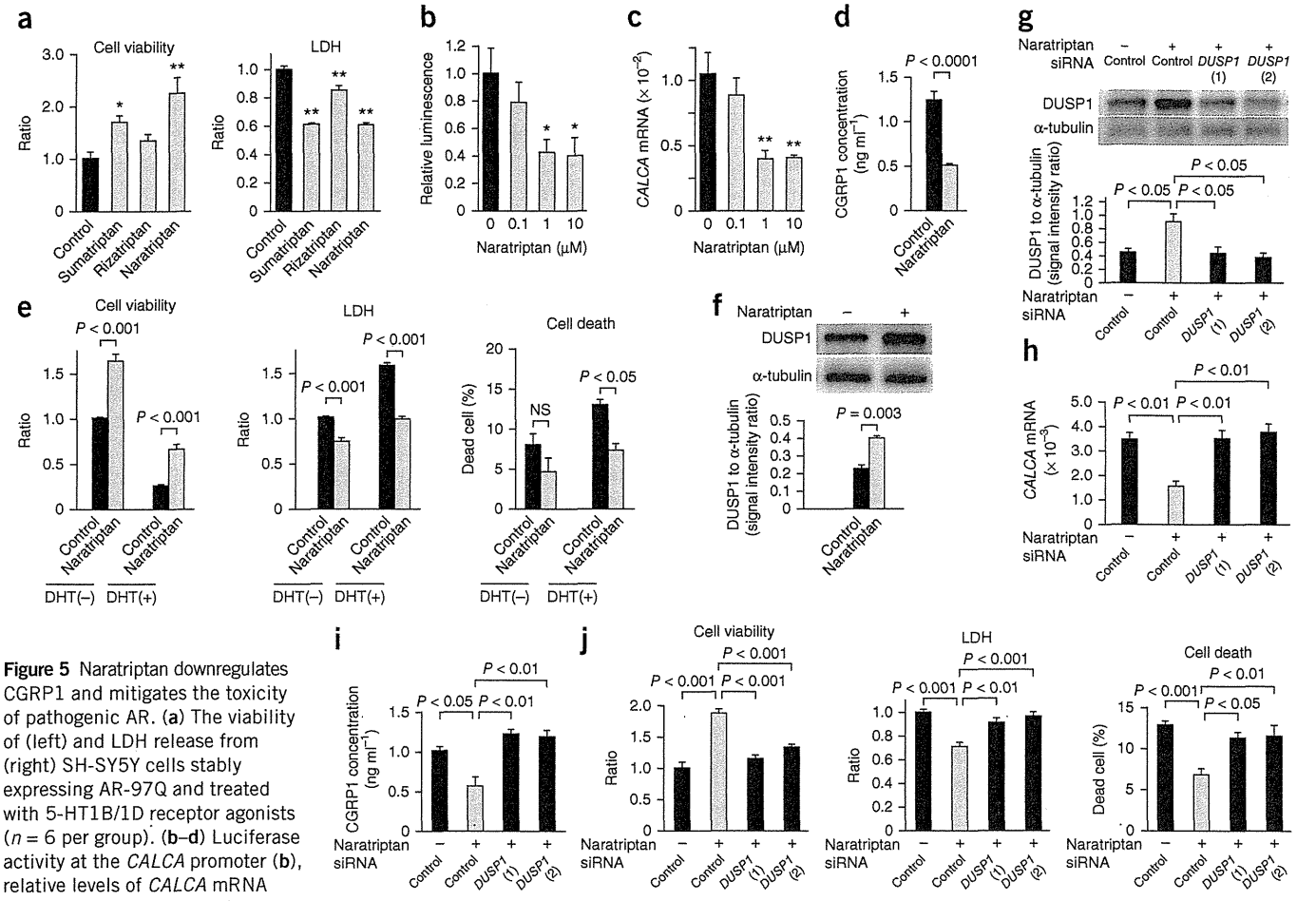

Figure 5 Naratriptan downregulates CGRP1 and mitigates the toxicity of pathogenic AR. (**a**) The viability of (left) and LDH release from (right) SH-SY5Y cells stably expressing AR-97Q and treated with 5-HT1B/1D receptor agonists ($n = 6$ per group). (**b–d**) Luciferase activity at the *CALCA* promoter (**b**), relative levels of *CALCA* mRNA relative to *GAPDH* mRNA (**c**) and concentration of CGRP1 (**d**) in SH-SY5Y cells that stably express AR-97Q and were treated with naratriptan ($n = 6$ per group). (**e**) The viability, LDH release and cell death of SH-SY5Y cells stably expressing AR-97Q that were treated with naratriptan and DHT ($n = 6$ per group). (**f**) Immunoblots (top) and relative signal intensities of DUSP1-immunoreactive bands (bottom) of SH-SY5Y cells stably expressing AR-97Q that were treated with or without naratriptan ($n = 3$ per group). (**g**) Immunoblots (top) and relative signal intensities of DUSP1-immunoreactive bands (bottom) of SH-SY5Y cells stably expressing AR-97Q that were transfected with the control or *DUSP1* siRNA and treated with or without naratriptan ($n = 3$ per group). (**h,i**) Relative levels of *CALCA* mRNA to *GAPDH* mRNA (**h**) and CRGP1 protein concentration (**i**) in SH-SY5Y cells stably expressing AR-97Q that were transfected with control or *DUSP1* siRNA and treated with naratriptan ($n = 3$ per group). (**j**) Viability, LDH release and cell death of SH-SY5Y cells stably expressing AR-97Q that were transfected with control or *DUSP1* siRNA and treated with naratriptan ($n = 6$ per group). The error bars indicate the s.e.m. $*P < 0.05$ and $**P < 0.01$ by ANOVA with Dunnett's test (**a–c**). Statistical analysis was performed using ANOVA with Tukey's test (**g–j**). NS, not significant.

of SBMA[30]. Therefore, we investigated the effects of naratriptan on the expression of CGRP1 and on polyglutamine-mediated cytotoxicity in neuronal cells. Administration of naratriptan reduced luciferase activity under control of the *CALCA* promoter as well as the mRNA and protein levels of CGRP1 in SH-SY5Y cells stably expressing AR-97Q (**Fig. 5b–d**). Naratriptan restored cell viability and suppressed the release of LDH, which is a marker of cytotoxicity, in cells treated with or without DHT, although the effects were more pronounced in the presence of DHT (**Fig. 5e**). Moreover, the effects of naratriptan on cell death were observable only when the SH-SY5Y cells expressing AR-97Q were treated with DHT (**Fig. 5e**).

Previous studies have suggested that 5-HT1B/1D receptor agonists suppress the expression of CGRP1 via the induction of DUSP1, a suppressor of the mitogen-activated protein kinase pathway[31]. We thus examined whether the neuroprotective effects of naratriptan are mediated by DUSP1. Naratriptan increased the expression of DUSP1 (**Fig. 5f**). SiRNA-mediated knockdown of *DUSP1* attenuated the effects of naratriptan on CGRP1 expression and neuroprotection in SH-SY5Y cells expressing AR-97Q (**Fig. 5g–j**). Pharmacological inhibition of DUSP1 with Ro-31-8220 in SH-SY5Y cells and primary motor neurons also attenuated naratriptan-mediated neuroprotection (**Supplementary Fig. 10a–g**). Furthermore, pharmacological inhibition of the 5-HT1B/1D receptor also inhibited the effects of naratriptan on CGRP1 expression and neuroprotection (**Supplementary Fig. 11a,b**), confirming that this receptor is involved in naratriptan-mediated suppression of the toxicity of the pathogenic AR.

We next investigated the effects of pharmacological stimulation of the 5-HT1B/1D receptor in a mouse model of SBMA. Oral administration of naratriptan improved grip strength and performance in the rotarod task of male AR-97Q mice in a dose-dependent manner as compared to vehicle-treated control AR-97Q mice (**Fig. 6a**). This pharmacological intervention also increased body weight and lifespan, although it showed no detectable effects on these phenotypes in wild-type mice (**Fig. 6a** and **Supplementary Fig. 12**). In agreement with the results of the cellular experiments, expression

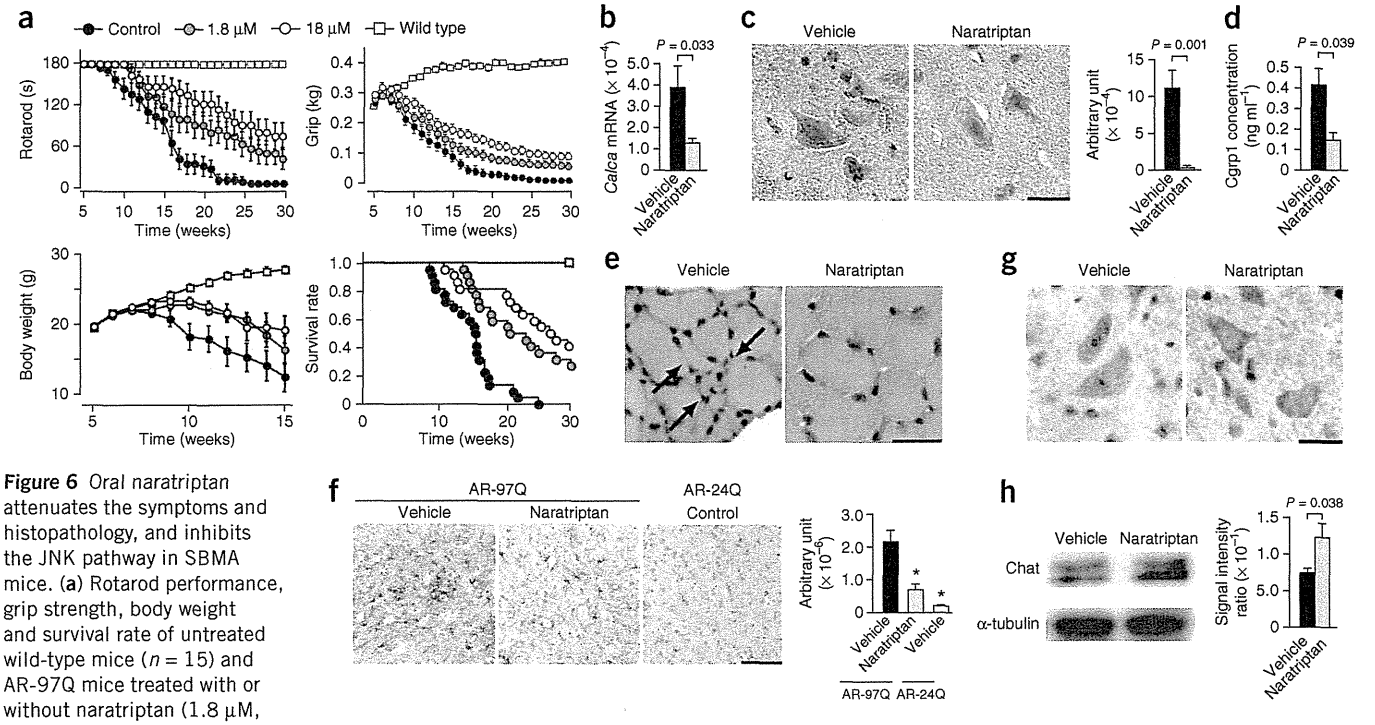

Figure 6 Oral naratriptan attenuates the symptoms and histopathology, and inhibits the JNK pathway in SBMA mice. (**a**) Rotarod performance, grip strength, body weight and survival rate of untreated wild-type mice ($n = 15$) and AR-97Q mice treated with or without naratriptan (1.8 μM, $n = 22$; 18 μM, $n = 22$). Significant differences were observed in all parameters between the untreated ($n = 22$) and 18 μM naratriptan–treated AR-97Q mice: $P < 0.01$ at 25 weeks (rotarod); $P < 0.01$ at 25 weeks (grip); $P < 0.05$ at 15 weeks (body weight); and $P < 0.0001$ (survival). (**b**) Relative levels of *Calca* mRNA to *Gapdh* mRNA in the spinal cords of AR-97Q mice treated with or without naratriptan ($n = 3$ per group). (**c**) Cgrp1 immunohistochemistry and intensity of immunoreactivity to Cgrp1 in spinal cords from AR-97Q mice treated with or without naratriptan ($n = 6$ per group). (**d**) The concentrations of Cgrp1 protein in the spinal cord of AR-97Q mice treated with or without naratriptan ($n = 3$ per group). (**e**) H&E staining of skeletal muscle from AR-97Q mice treated with or without naratriptan. (**f**) Gfap immunohistochemistry (left) and intensity of immunoreactivity to Gfap (right) in spinal cord sections from AR-97Q mice treated with or without naratriptan ($n = 6$ per group). (**g**) ChAT immunohistochemistry in spinal cord sections from AR-97Q mice treated with or without naratriptan. (**h**) Immunoblots and relative intensities of ChAT-immunoreactive bands of spinal cords from AR-97Q mice treated with or without naratriptan ($n = 6$ per group). The scale bars indicate 20 μm (**c**,**g**) or 50 μm (**e**,**f**). The error bars indicate the s.e.m. *$P < 0.01$ by ANOVA with Dunnett's test (**f**).

of *Calca* was lower in the spinal cords of male AR-97Q mice treated with naratriptan as compared to vehicle-treated controls (**Fig. 6b**). Immunohistochemistry and ELISA revealed that naratriptan suppressed expression of Cgrp1 at the protein level in the spinal motor neurons of SBMA mice (**Fig. 6c,d**). Histopathological analyses indicated that oral naratriptan also reduced muscle wasting, suppressed reactive astrogliosis and increased expression of ChAT in the spinal motor neurons of AR-97Q mice (**Fig. 6e–h**).

Naratriptan suppresses the JNK pathway

To elucidate the molecular basis for the neuroprotection induced by naratriptan, we investigated the effects of this drug on the activity of the JNK pathway. Naratriptan treatment decreased the phosphorylation of c-Jun in SH-SY5Y cells stably expressing AR-97Q and treated with DHT (**Supplementary Fig. 13a,b**). Immunoblotting and immunohistochemistry showed that oral naratriptan also reduced the phosphorylation of c-Jun in the spinal cords of male AR-97Q mice (**Supplementary Fig. 14a,b**). Since the activation of JNK by pathogenic AR disrupts axonal transport, which contributes to the pathogenesis of SBMA[17,32], we investigated the effects of naratriptan on axonal transport. Naratriptan increased the number of motor neurons labeled with FluoroGold, a tracer used to measure retrograde axonal transport in mice (**Supplementary Fig. 15a,b**). As for the safety of naratriptan, we did not observe any adverse effects of oral treatment with naratriptan at 18 μM for 8–10 weeks on liver or renal function (**Supplementary Fig. 15c**).

DISCUSSION

Here we showed that the pathogenic AR protein dysregulates transcription in a mouse model of SBMA before the onset of motor impairment. Among the disease-specific transcriptional changes, CGRP1 was upregulated as the disease progressed and was also found to be upregulated in humans with SBMA and in a cellular model of SBMA. Alterations of gene expression have been demonstrated by microarray analyses of human postmortem specimens and in cellular and animal models of polyglutamine diseases, suggesting that transcriptional dysregulation is central to the pathogenesis of polyglutamine diseases that is independent of the context of the causative protein[22,33,34]. We found that pathogenic AR proteins increase activity at the *CALCA* gene promoter, which indicates that the transcription of CGRP1 is upregulated by pathogenic AR in SBMA.

CGRP1 is known to be upregulated upon neuronal injury, which suggests a potential neuroprotective role of this molecule[35]. On the contrary, elevated expression of CGRP1 is reported to be correlated with increased vulnerability of motor neurons in a mouse model of amyotrophic lateral sclerosis linked to a mutation in the gene encoding superoxide dismutase 1 (SOD1)[36]. Depletion of *Calca*, however, has no effect on the disease progression in mutant *Sod1* mice, suggesting that the basal expression of CGRP1 has neither neurotoxic nor neuroprotective effects[37]. Alternatively, other molecules may overwhelm the effects of CGRP1 on motor neuron degeneration in amyotrophic lateral sclerosis. In contrast, our study shows that increased expression of CGRP1 reduces the viability and induces